iScience

CellPress
OPEN ACCESS

Article

Distinct GABAergic modulation of timing-dependent LTP in CA1 pyramidal neurons along the longitudinal axis of the mouse hippocampus

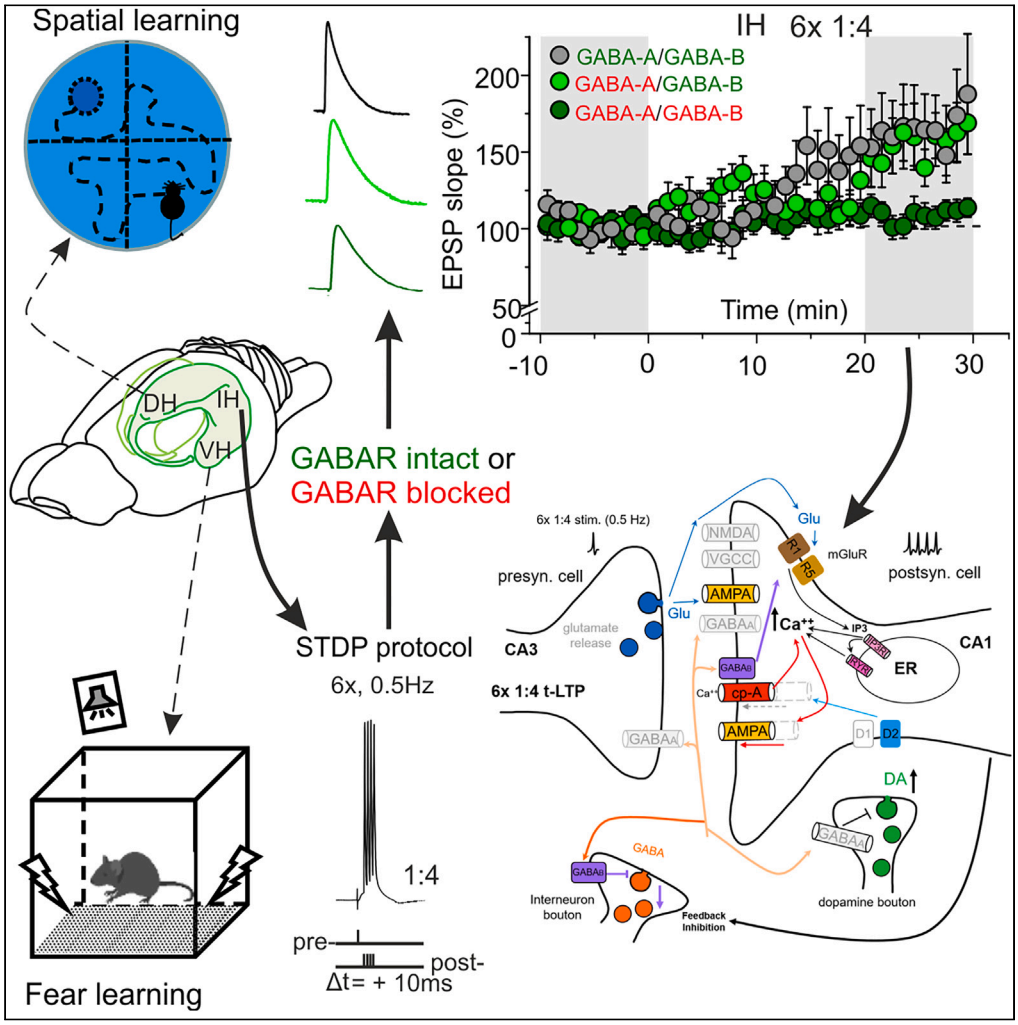

Babak Khodaie,
Elke Edelmann,
Volkmar Leßmann

volkmar.lessmann@med.ovgu.de

Highlights

Low repeat timing-LTP is easier to induce in ventral than in dorsal hippocampus

Six repeat theta-burst t-LTP (6× 1:4 t-LTP) is insensitive to $GABA_A$ mediated inhibition

6× 1:4 t-LTP requires intact $GABA_B$ receptor mediated inhibition

t-LTP expression varies along dorsoventral hippocampal axis and with induction protocol

Khodaie et al., iScience 27, 109320
March 15, 2024
https://doi.org/10.1016/j.isci.2024.109320

iScience

CellPress
OPEN ACCESS

Article

Distinct GABAergic modulation of timing-dependent LTP in CA1 pyramidal neurons along the longitudinal axis of the mouse hippocampus

Babak Khodaie,[1,3] Elke Edelmann,[1,2,3] and Volkmar Leßmann[1,2,3,4,5,*]

SUMMARY

Synaptic plasticity in the hippocampus underlies episodic memory formation, with dorsal hippocampus being instrumental for spatial memory whereas ventral hippocampus is crucial for emotional learning. Here, we studied how GABAergic inhibition regulates physiologically relevant low repeat spike timing-dependent LTP (t-LTP) at Schaffer collateral-CA1 synapses along the dorsoventral hippocampal axis. We used two t-LTP protocols relying on only 6 repeats of paired spike-firing in pre- and postsynaptic cells within 10 s that differ in postsynaptic firing patterns. $GABA_A$ receptor mechanisms played a greater role in blocking 6× 1:1 t-LTP that recruits single postsynaptic action potentials. 6× 1:4 t-LTP that depends on postsynaptic burst-firing unexpectedly required intact $GABA_B$ receptor signaling. The magnitude of both t-LTP-forms decreased along the dorsoventral axis, despite increasing excitability and basal synaptic strength in this direction. This suggests that GABAergic inhibition contributes to the distinct roles of dorsal and ventral hippocampus in memory formation.

INTRODUCTION

The hippocampus and its associated medial temporal lobe structures constitute a complex network of excitatory and inhibitory synapse microcircuits to process learning and memory formation. Early on, the hippocampus was divided into three distinguishable compartments, including dorsal hippocampus (DH), intermediate hippocampus (IH), and ventral hippocampus (VH) parts along its longitudinal axis that were correlated with the formation of different types of memories.[1,2] More recent studies demonstrated a genetic, morphological, and functional diversity of CA1 pyramidal cell (CA1 PC) circuits along the longitudinal axis of the hippocampus,[3] where the DH has been associated especially with spatial memory tasks,[4] while the VH is more important for processing of emotional memories (see e.g., Meis et al.[5]). Studies focusing on CA1 PC structural and functional properties confirmed the existence of distinguishable regions along the longitudinal axis of the hippocampus based on differential gene expression, intrinsic physiological characteristics, and firing properties in the rat hippocampus.[6] This diversity of CA1 circuits along the longitudinal axis is most likely generated by distinct expression profiles of membrane receptors and ion channels, as well as different glutamatergic and neuromodulatory inputs projecting from discernable cortical and subcortical regions to DH, IH, and VH, respectively. These differences of CA1 circuits are paralleled by distinct efficacy for induction of long-term potentiation (LTP) at Schaffer collateral-CA1 (SC-CA1) synapses, with higher LTP magnitudes in rat DH compared to VH.[7,8] This structural, functional, and gene expression disparity of CA1 PC circuits along the longitudinal axis of the hippocampus suggests that distinct molecular and cellular mechanisms for induction and expression of LTP might contribute to the processing of information in DH, IH, and VH also in mice.

Previous studies have emphasized that inhibitory synaptic inputs play a substantial role in shaping synaptic plasticity and integration of different synaptic inputs to CA1 PCs, explaining the importance of excitatory and inhibitory balance for information processing in synaptic circuits.[9,10] In this respect, Dubovyk & Manahan-Vaughan[7] revealed non-uniform expression of $GABA_A$ and $GABA_B$ receptors along the longitudinal axis of the hippocampus in rats, showing a higher expression of $GABA_A$ receptors in DH compared to higher $GABA_B$ receptor expression in VH. Such specificity in GABA receptor expression might account for region specific synaptic encoding mechanisms in DH vs. VH CA1 circuits. Interestingly, it was shown previously in rat prefrontal cortex that $GABA_A$ and $GABA_B$ receptors differentially modulate dopamine release.[11] Given the important role dopamine plays in regulating synaptic plasticity in hippocampal circuits (reviewed, e.g., in Edelmann and Lessmann[12]; Pawlak et al.[13]; Brzosko et al.[14]), different GABAergic mechanisms might exert regulation of LTP through modulating dopamine release. In fact, both extracellular dopamine levels[15] and expression of dopamine receptor subtypes show gradual changes along the longitudinal axis of the rat hippocampus.[7,16] Putting all these pieces of information together, the distinct interaction of inhibitory GABAergic

[1]Institut für Physiologie, Otto-von-Guericke-Universität (OVGU), Medizinische Fakultät, 39120 Magdeburg, Germany
[2]Center for Behavioral Brain Sciences, 39104 Magdeburg, Germany
[3]OVGU International ESF-funded Graduate School ABINEP, 39104 Magdeburg, Germany
[4]DZPG (German Center of Mental Health), partner site Halle/Jena/Magdeburg (CIRC), Magdeburg, Germany
[5]Lead contact
*Correspondence: volkmar.lessmann@med.ovgu.de
https://doi.org/10.1016/j.isci.2024.109320

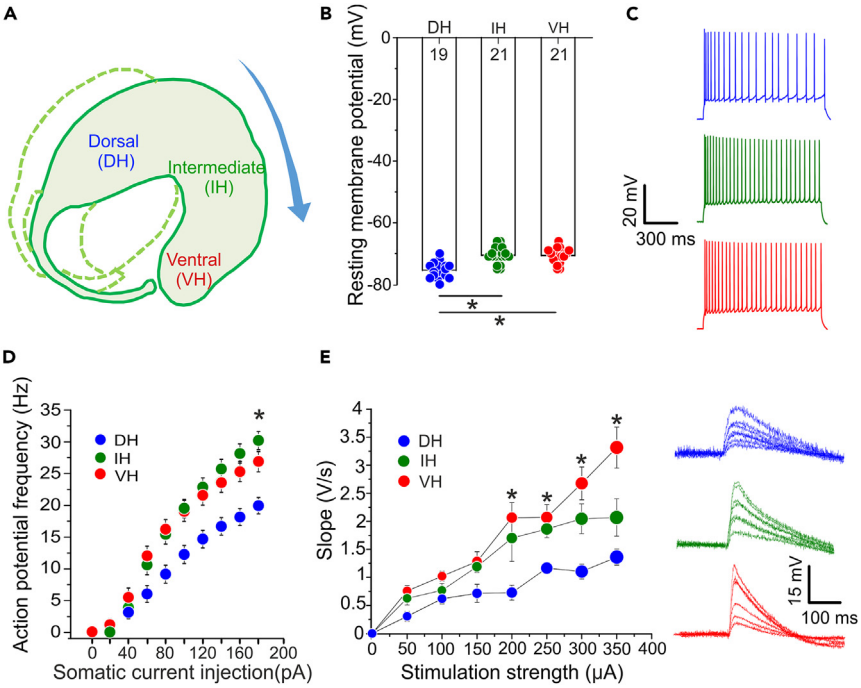

Figure 1. Basal electrical and synaptic properties of CA1 pyramidal neurons along the longitudinal axis of the hippocampus

(A) Schematic graph illustrates different hippocampal poles along longitudinal axis in rodents.

(B) Resting membrane potential of pyramidal cells (PCs) in DH (n = 19/N = 10), IH (n = 21/N = 11) and VH (n = 21/N = 10), is more depolarized in IH and VH compared to DH.

(C) Recording in current clamp (CC) mode at −70 mV holding potential. Action potential (AP) firing in CA1 neurons in response to 180 pA somatic current injection (1 s duration) in DH (blue), IH (green), and VH (red).

(D) AP frequency along the dorsoventral axis of the hippocampus in response to different step current injections, indicating higher intrinsic excitability of CA1 PCs in both IH and VH compared to DH PCs. Digits in the bars represent the number of recorded cells. Inset: Original traces of single cell responses to different depolarization steps.

(E) Synaptic input-output curves at Schaffer collateral (SC) inputs to CA1 are steeper in VH and IH than in DH, indicating higher baseline synaptic strength toward the VH pole. Original traces of individual cells at different stimulation intensities are shown on the right. Data are shown as mean ± SEM. Scale bars are shown in the figures. Multiple comparisons were performed with ANOVA using post hoc Tukey's test. See also Figures S1 and S2.

and excitatory synaptic inputs and a gradient of neuromodulator signaling could account for specific LTP induction and expression mechanisms from the dorsal to the ventral pole of the hippocampus. However, such differences in LTP expression mechanisms have not yet been investigated for SC-CA1 LTP.

Spike timing-dependent plasticity (STDP) experimentally mimics the Hebbian learning rule, where precise millisecond timing delays of presynaptic and postsynaptic firing of action potentials (APs) increase or decrease synaptic strength.[17–30] To generate a memory trace, several seconds of such ongoing slightly delayed AP firing in pre- and postsynaptic cells is required and needs to be actively shaped by appropriate GABAergic and glutamatergic synaptic activity within the memory encoding synaptic circuit.

Here, we aimed at testing whether several seconds of STDP-like AP firing at SC-CA1 synapses is converted by different mechanisms into timing-dependent (t)-LTP along the longitudinal axis of the hippocampus. Patch clamp recorded CA1 neurons were subjected to canonical (i.e., 1 presynaptic AP paired with 1 postsynaptic AP; 1:1) or burst t-LTP protocols (1:4), repeated six times at 0.5 Hz in acute mouse hippocampal slices taken from DH, IH, or VH.[31,32] Specifically, we investigated the role of $GABA_A$ and $GABA_B$ receptor mediated synaptic inhibition on induction and expression of 6× 1:1 and 6× 1:4 t-LTP.

Our results indicate a complex association of excitatory and inhibitory responses depending on stimulation protocols (canonical or burst t-LTP) and studied region (DH, IH, or VH). While the 6× 1:1 protocol lost its dependency on GABAergic signaling to induce robust t-LTP from DH to VH pole, our 6× 1:4 protocol mainly depended on active $GABA_BR$ signaling during t-LTP induction.

RESULTS

Distinct basal electrophysiological properties of CA1 pyramidal neurons along the longitudinal axis of the hippocampus

Using whole-cell patch clamp recording we measured basal electrical and synaptic properties of postsynaptic CA1 pyramidal cells (PCs) located along the longitudinal axis of the hippocampus, (Figure 1A). If not stated otherwise, all recordings were performed in the presence of the $GABA_A$ receptor inhibitor picrotoxin. The resting membrane potential (RMP) of CA1 PCs was significantly more depolarized

in IH and VH CA1 PCs compared to the DH (IH: −70.52 ± 0.57 mV, and VH: −70.62 ± 0.50 mV vs. DH: −75.37 ± 0.57 mV; ANOVA $F_{(2,58)}$ = 24.91 $p < 0.0001$, post hoc Tukey-test $p < 0.0001$; Figure 1B). Next, we determined AP frequencies induced by somatically injected step currents (Figures 1C and 1D). At 180 pA current injection, the AP frequency was 30.19 ± 1.36 Hz in IH, 26.90 ± 1.46 Hz in VH, and 19.95 ± 1.22 Hz in DH CA1 PCs, showing a significantly higher AP frequency in both IH and VH compared to DH (ANOVA $F_{(2,58)}$ = 14.38 $p < 0.0001$, post hoc Tukey-test for IH vs. DH $p < 0.0001$, and VH vs. DH $p = 0.002$). Subsequently, intrinsic neuronal excitability was determined using measurement of the rheobase, i.e., the minimal current injection (at 10 ms step length) needed to elicit an AP.[33] The rheobase was 155.24 ± 11.54 pA in IH, and 139.05 ± 10.55 pA in VH, compared to 188.42 ± 13.62 pA in DH CA1 PCs, indicating significantly higher rheobase in DH compared to VH PCs (Kruskal–Wallis test $H_{(3)}$ = 8.93; $p = 0.011$, Figure S1). To determine the strengths of Schaffer collateral (SC) synaptic inputs to CA1 PCs along the longitudinal axis of the hippocampus, we measured input-output curves (I/O curves; i.e., strength of SC extracellular stimulation current vs. slope of postsynaptic EPSPs). At 200 μA stimulation intensity, EPSP slopes were significantly different in VH compared to DH CA1 PCs (VH: 2.06 ± 0.27 V/s, IH: 1.70 ± 0.42 V/s and DH: 0.73 ± 0.13 V/s; ANOVA $F_{(2,\ 22)}$ = 5.96; $p = 0.0085$ post hoc Tukey-test, $p = 0.0085$; Figure 1E, compare Figure S2). Starting at 250 μA stimulation intensity, both VH and IH showed significantly larger responses compared to DH (VH: 2.07 ± 0.22 V/s, IH: 1.86 ± 0.15 V/s and DH: 1.16 ± 0.06 V/s; ANOVA $F_{(2,\ 22)}$ = 9.52; $p = 0.0011$, post hoc Tukey-tests for VH vs. DH $p = 0.0012$, and for IH vs. DH $p = 0.011$). Thus, mouse VH and IH have more depolarized RMP, fire higher frequencies of APs, and show higher magnitudes of evoked excitatory postsynaptic responses at SC-CA1 synapses compared to DH.

Distinct release probability of SC-CA1 synapses along the longitudinal axis of the hippocampus

Previous studies in rats suggested distinct presynaptic release probability at SC-CA1 synapses along the dorsoventral axis of the hippocampus.[7,34] Changes in the EPSC paired-pulse ratio (PPR) are commonly used as a convenient method to measure release probability,[35] with high PPR indicating a low transmitter release probability in response to the first presynaptic stimulation. In our recordings, the mean PPR in CA1 PCs was 2.11 ± 0.15 in DH, 1.79 ± 0.12 in IH, and 1.68 ± 0.11 in VH, showing a significantly smaller PPR in VH compared to DH (ANOVA $F_{(2,\ 57)}$ = 3.16; $p = 0.05$, post hoc Tukey-test, $p = 0.046$; Figure 2B). As an additional measure of glutamate release probability, we analyzed amplitude and frequency of putative miniature excitatory postsynaptic currents (pmEPSCs) in CA1 PCs (Figures 2C–2E). CA1 PCs in IH and VH showed significantly higher mean pmEPSC amplitudes (IH: 11.91 ± 0.77 pA; VH: 11.65 ± 0.61 pA) than DH PCs (DH: 9.64 ± 0.31 pA; ANOVA $F_{(2,\ 26)}$ = 6.19; $p = 0.0063$; post hoc Tukey-test for IH vs. DH: $p = 0.013$, and VH vs. DH: $p = 0.029$; Figure 2D left). Likewise, we also observed a significantly different cumulative pmEPSC amplitude distribution in DH compared to VH and IH (Kruskal–Wallis test $H_{(3)}$ = 232; $p < 0.0001$; Figure 2D right). We then determined mean pmEPSC frequencies along the longitudinal axis, and found significantly lower pmEPSC frequencies in DH CA1 PCs (0.25 ± 0.03 Hz) compared to IH and VH (IH: 0.85 ± 0.15 Hz, VH: 0.6 ± 0.14 Hz; ANOVA $F_{(2,\ 26)}$ = 9.67; $p = 0.0007$; post hoc Tukey-test $p = 0.0006$, and $p = 0.046$ respectively; Figure 2E left). Accordingly, also cumulative pmEPSC inter-event interval (IEI) distribution indicated a significantly lower presynaptic release probability in DH compared to IH and VH (Kruskal–Wallis test $H_{(3)}$ = 840.9; $p < 0.0001$; Figure 2E right). These results are consistent with significantly decreased charge transfer of pmEPSCs in DH vs. IH (compare Figure S7).

Taken together these results indicate that glutamate release probability and magnitude of postsynaptic responses at SC-CA1 synapses are significantly smaller in DH compared to both IH and VH.

Gradient of t-LTP magnitude at Schaffer collateral-CA1 synapses along the longitudinal axis of the hippocampus

For t-LTP induction we used two different recently established physiologically relevant low repeat (6 times; 6×) t-LTP protocols consisting of coincident pairing of a single presynaptic AP with either one (1:1, Figure 3A) or four (1:4, Figure 3B) postsynaptic APs.[31] Typical original single cell EPSP time courses for both protocols in DH and VH are shown in Figures 3C and 3D. To avoid observation of ongoing synaptic network activity by spontaneous AP firing of CA3 neurons, SC fibers were cut in CA2. Both protocols induced successful t-LTP compared to negative controls (0:0) in all studied regions along the longitudinal axis of the hippocampus (Figure S3). Interestingly, the magnitude of t-LTP induced by 6× 1:1 stimulation was significantly higher only in CA1 PCs of the DH (203.20 ± 17.26%, (n = 10/N = 7) compared to VH (135.09 ± 7.41%, (n = 11/N = 7); ANOVA $F_{(2,\ 27)}$ = 5.59 $p = 0.0093$, post hoc Tukey-test $p = 0.007$; Figure 3E), whereas 6× 1:1 stimulation in IH induced an intermediate magnitude of t-LTP (168.50 ± 18.92%, (n = 9/N = 6)). As shown in Figure 3F, the 6× 1:4 paradigm showed a similar efficacy to induce t-LTP as the 6× 1:1 paradigm. Thus, 6× 1:4 t-LTP magnitudes were 184.54 ± 14.10% in DH (n = 11/N = 7), 162.55 ± 9.70% in IH (n = 11/N = 6), and 146.77 ± 12.74% in VH (n = 11/N = 6), showing a non-significant reduction in t-LTP magnitude from the DH to VH (Kruskal–Wallis test, $H_{(3)}$ = 3.838; $p = 0.147$).

Thus, while CA1 PCs in VH and IH are more excitable, show higher glutamate release probability and larger pmEPSC amplitudes (compare Figures 1 and 2) the CA1 PCs in DH show a higher efficacy of t-LTP. The results for t-LTP in response to the two STDP paradigms applied under diverse conditions for GABAergic inhibition, and their effects on PPR, AMPA/NMDA receptor ratios, and the coefficient of variation analysis are summarized for DH, IH, and VH in Table S1 (supplemental information).

Differential expression loci of t-LTP induced by low repeat 1:1 and 1:4 paradigms along the longitudinal axis of the hippocampus

We previously reported distinct loci of expression of low repeat (6×) 1:1 and 1:4 paradigms at SC-CA1 synapses in IH in the presence of the $GABA_AR$ inhibitor picrotoxin.[31] Given the distinct magnitudes of t-LTP from DH to VH, we next asked whether the loci of expression of 6× 1:1 and 6× 1:4 t-LTP differ along the dorsoventral axis of the hippocampus under $GABA_AR$ blockade. To this aim, we analyzed the changes in PPR

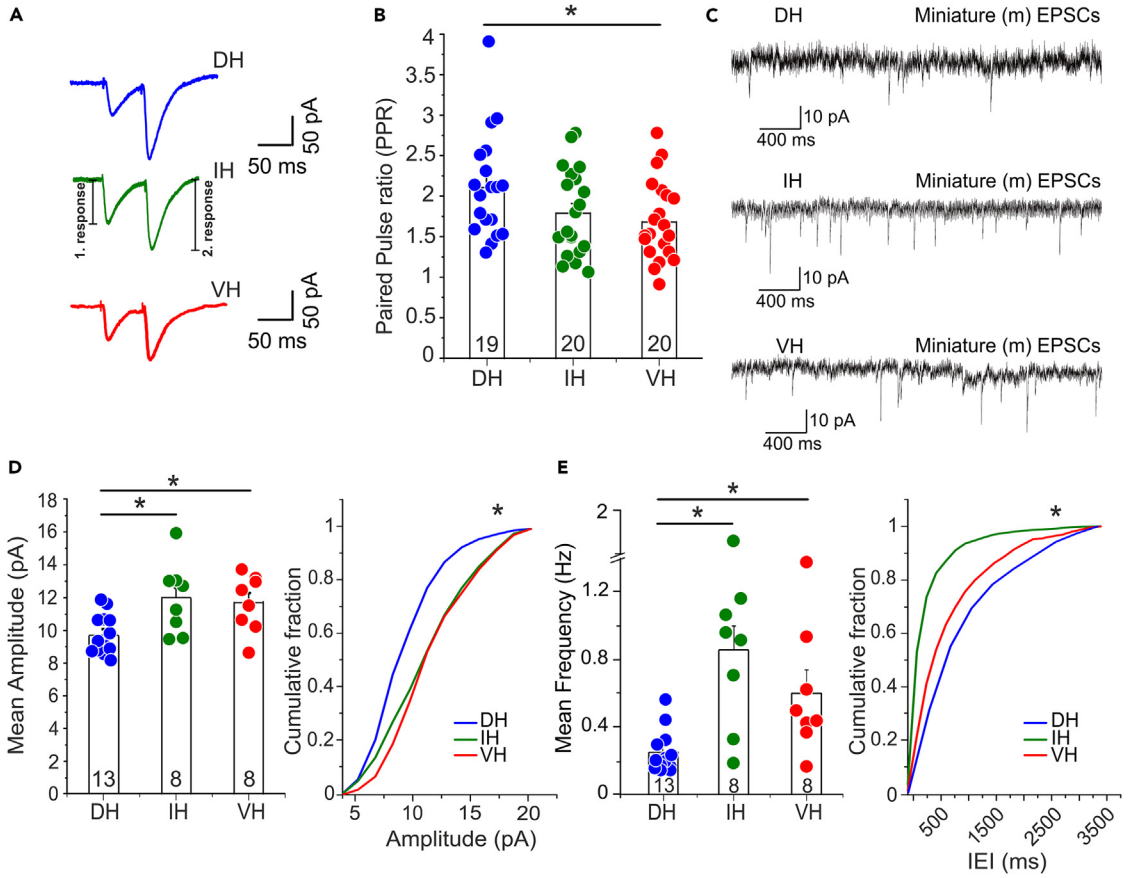

Figure 2. SC-CA1 synaptic transmission along the longitudinal axis of the hippocampus shows regional differences

All recordings performed in voltage clamp (VC) mode at −70 mV holding potential in the presence of picrotoxin, (A) Original traces representing postsynaptic cell responses to paired SC stimulation with an interval of 50 ms. 2nd peak current response divided by 1st response was used to calculate PPR.

(B) PPR is significantly higher in DH PCs (n = 19/N = 10) compared to VH PCs (n = 20/N = 10), indicating higher release probability at the VH pole, while IH PC (n = 20/N = 9) release probability lies in between.

(C) Original traces of recorded miniature (m) EPSCs along the longitudinal axis.

(D and E) Mean amplitudes, frequencies and cumulative fraction of inter-event intervals (IEI) of along the longitudinal axis (DH: n = 13/N = 5; IH: n = 8/N = 4, and VH: n = 8/N = 5). Each circle represents an individual cell. Data are shown as mean ± SEM. Scale bars are shown in the figures. Multiple comparisons were performed with ANOVA using post hoc Tukey's test and for cumulative fraction Kruskal–Wallis test. Compare Figure S2.

before, and 30 min after t-LTP induction by two successively evoked EPSCs elicited at 50 ms interstimulus interval (Figures 4A and 4B; compare Figures 2A and 2B). Of note, a reduction in PPR after t-LTP induction is considered to indicate presynaptically expressed synaptic plasticity (i.e., increased glutamate release). Following successful t-LTP induction with the 6× 1:1 paradigm, the mean PPR recorded in CA1 PCs of IH was significantly reduced (before t-LTP: 2.19 ± 0.24, after t-LTP: 1.53 ± 0.17; paired Student's *t* test, $t_{(8)} = 4.338$, p = 0.0025). Similarly, in VH PCs we found a significant decrease in PPR after 6× 1:1 t-LTP induction (before: 1.82 ± 0.2, after: 1.30 ± 0.09; paired Student's *t* test, $t_{(10)} = 3.72$, p = 0.004; Figure 4A). However, in DH there was no change in PPR following 6× 1:1 t-LTP induction (before: 2.22 ± 0.24, after: 2.16 ± 0.21, paired Student's *t* test, $t_{(9)} = 0.22$; p = 0.827). For 6× 1:4 t-LTP we did not observe a significant change in PPR throughout the hippocampus (DH before: 2.18 ± 0.17, after: 2.42 ± 0.16, paired Student's *t* test, $t_{(9)} = 1.042$; p = 0.32, IH before: 1.83 ± 0.16, after: 1.74 ± 0.15, paired Student's *t* test, $t_{(10)} = 0.43$, p = 0.67, VH before: 1.97 ± 0.16, after: 1.71 ± 0.12, paired Student's *t* test, $t_{(10)} = 1.58$, p = 0.14; Figure 4B). We could show previously that the analysis of pmEPSC frequencies and amplitudes before vs. after successful induction of t-LTP confirmed presynaptic versus postsynaptic expression as determined by PPR analysis.[31,32] Therefore, we did not re-confirm our PPR results with pmEPSC analysis here again.

To investigate the contribution of postsynaptic expression mechanisms to both t-LTP paradigms, we next analyzed the changes in AMPA and NMDA receptor (R)-mediated current ratios after successful t-LTP induction with 6× 1:1 and 6× 1:4 paradigms, compared to non-stimulated negative controls (0:0). Of note, due to distinct expression of NMDAR subunits (GluN2A and GluN2B) along the longitudinal axis of rat hippocampus,[7] NMDAR-mediated currents at SC-CA1 synapses in the VH (GluN2A < GluN2B) decay three times more slowly than in the DH (GluN2A > GluN2B).[36,37] While AMPAR-mediated peak EPSCs were measured at a holding potential of −70 mV, the NMDAR-mediated

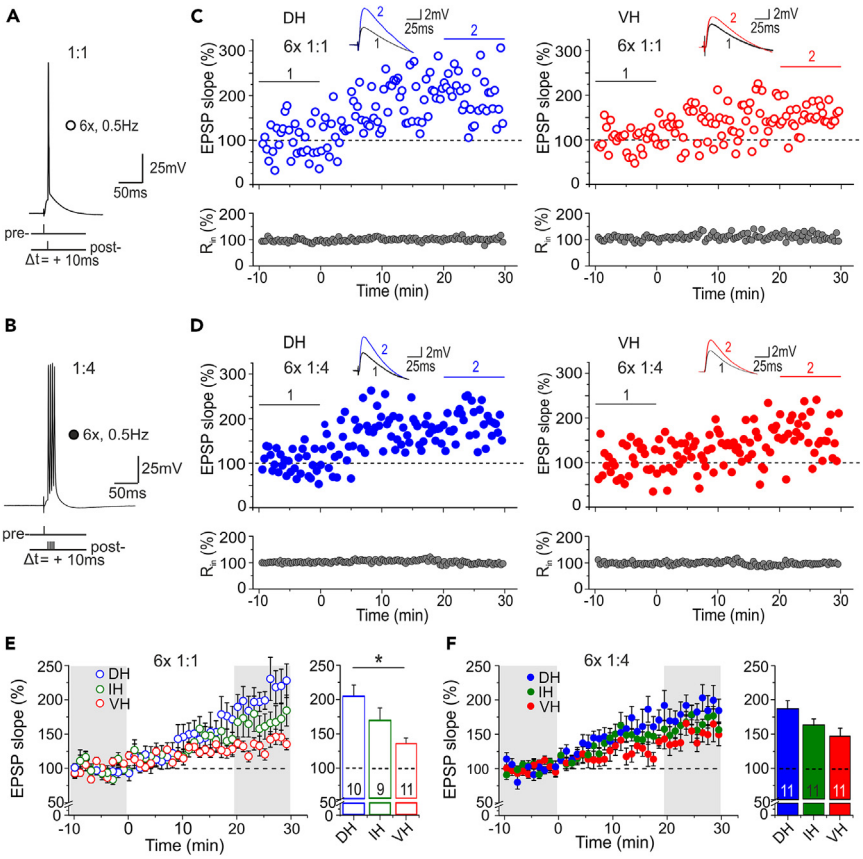

Figure 3. Comparison of t-LTP magnitude at SC-CA1 inputs induced by low-repeat canonical and burst STDP protocols along the longitudinal axis of the hippocampus

All recordings were performed in CC mode at −70 mV holding potential in the presence of picrotoxin, (A) Original voltage trace for 6× 1:1 and (B) 6× 1:4 protocols.

(C) Typical time course of 6× 1:1 t-LTP for single cells in DH (left, open blue circles), and VH (right, open red circles).

(D) Typical time course of 6× 1:4 t-LTP for DH (left, closed blue circles), and VH (right, closed red circles). At the top of the graphs, the inserts represent the EPSPs during baseline recording (1) and 20 min after STDP protocol (2).

(E) Averaged time courses of t-LTP revealed a significantly weaker t-LTP induced with the 6× 1:1 paradigm in VH (n = 11/N = 7) compared to DH (n = 10/N = 7), while IH (n = 9/N = 6) showed an intermediate t-LTP magnitude.

(F) t-LTP magnitude induced by 6× 1:4 protocol along the dorsoventral axis shows no statistically significant difference between DH PCs (n = 11/N = 7) to IH (n = 11/N = 6) and VH PCs (n = 11/N = 6), although there was a gradient in t-LTP magnitude along the longitudinal axis. The average magnitude of t-LTP is shown in the bar graphs. Data are shown as mean ± SEM. Multiple comparisons were performed with ANOVA using post hoc Tukey's test. Scale bars are shown in the figures. See also Figures S3 and S10.

current components were read out at −20 mV holding potential at different time points of the decaying EPCSs in DH, IH, and VH (see STAR Methods section and Figure 4C). Our analysis of the AMPAR/NMDAR current ratio indicated a statistically significant increase in AMPAR- versus NMDAR-mediated EPSC component after 6× 1:4 but not 6× 1:1 t-LTP induction in IH CA1 PCs (neg. controls (0:0): 6.16 ± 0.75, 6× 1:1: 5.69 ± 0.52, and 6× 1:4: 9.77 ± 1.29; Kruskal–Wallis test, $H_{(3)} = 10.47$, p = 0.0053; Figure 4C, middle). A similar effect was observed in VH (0:0: 6.77 ± 1.15, 6× 1:1: 5.32 ± 0.7, and 6× 1:4: 9.94 ± 0.83; ANOVA $F_{(3, 30)} = 10.26$, p = 0.0059; Figure 4C, right). Interestingly, in DH PCs the AMPAR/NMDAR current ratio was significantly increased by successful 6× 1:4, and also 6× 1:1 t-LTP induction, compared to non-STDP stimulated control cells (0:0: 4.67 ± 0.73, 6× 1:1: 9.07 ± 0.48, and 6× 1:4: 9.49 ± 1.24; ANOVA $F_{(2, 27)} = 5.55$, p = 0.009, post hoc Tukey-test for 0:0 vs. 6× 1:1 p = 0.02 and for 0:0 vs. 6× 1:4 p = 0.01; Figure 4C, left). Overall, these results are consistent with postsynaptic changes after 6× 1:4 t-LTP in IH, VH and DH, while only in DH CA1 PCs postsynaptic changes were seen also after induction of 6× 1:1 t-LTP. Of note, it has been shown previously that incorporation of new GluA1 containing AMPARs into the postsynaptic membrane accounts for the increased AMPAR/NMDAR current ratio observed in response to the induction of (t-)LTP (see[38] and.[31]

As a further measure for the expression locus of t-LTP, we performed coefficient of variation (CV) analysis of evoked EPSPs (see e.g.,[32,39,40] The CV is a readout of presynaptic variability of transmitter release upon repeated stimulation, normalized by the mean.[41,42] When t-LTP is expressed presynaptically, CV after t-LTP should decrease compared to CV before LTP induction. While results for CV analysis corroborate

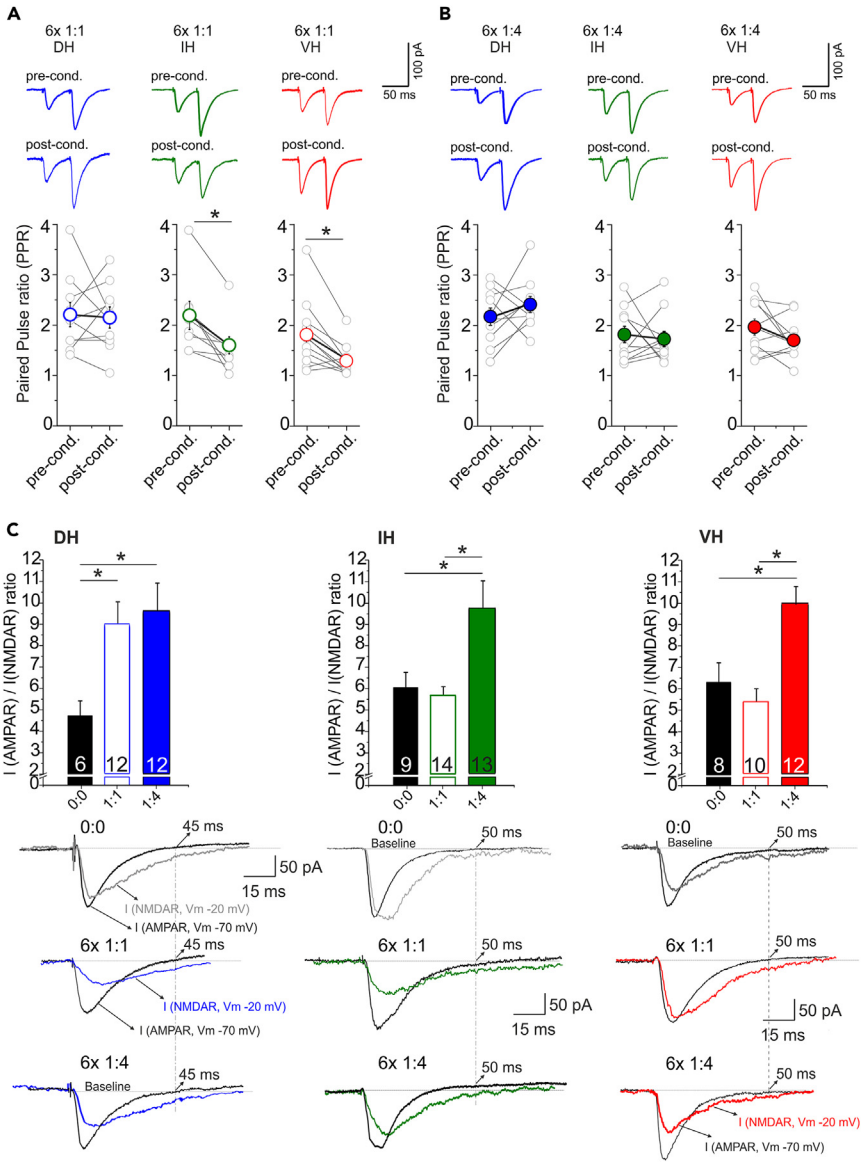

Figure 4. Diverse expression loci of SC-CA1 t-LTP induced by low repeat 1:1 and 1:4 paradigms along the longitudinal axis of the hippocampus

All recordings performed in VC mode at −70 or −20 mV holding potential in the presence of picrotoxin, A) Paired pulse ratio (PPR) calculated before (pre-cond.) and 30 min after (post-cond) 6× 1:1 t-LTP induction in the same cell (DH: n = 10/N = 7; IH: n = 9/N = 5, and VH: n = 11/N = 6), showing significant changes in PPR after 6× 1:1 t-LTP induction in IH and VH. B) PPR measurement after 6× 1:4 t-LTP revealed no significant changes in presynaptic release probability in either of the studied regions (DH: n = 10/N = 7; IH: n = 11/N = 6, and VH: n = 11/N = 6).

(C) Upper panel: ratio of AMPA/NMDA receptor–mediated currents (AMPAR: peak current at −70 mV; NMDAR: current amplitude 50 ms (in IH and VH) and 45 ms (in DH) after start of EPSCs, recorded at −20 mV) for negative controls (0:0: in DH; n = 6/N = 5; in IH: n = 9/N = 7; in VH: n = 8/N = 6), after successful induction of t-LTP with both low repeat paradigms in DH (6× 1:1: n = 12/N = 7; 6× 1:4: n = 12/N = 6), in IH (6× 1:1: n = 14/N = 10; 6× 1:4: n = 13/N = 8), and VH (6× 1:1: n = 10/N = 8; 6× 1:4: n = 12/N = 9). An increased AMPAR/NMDAR current ratio could be seen after both 6× 1:1 and 6× 1:4 t-LTP in DH CA1 PCs, suggesting postsynaptic changes following successful t-LTP for both paradigms. In IH and VH, AMPAR/NMDAR current ratio increased only after 6× 1:4 t-LTP, speaking in favor of a postsynaptic change. Lower panel: original traces of AMPAR-mediated currents recorded at −70 mV holding potential (black) and NMDAR (in gray: 0:0; blue: 6× 1:1, and red: 6× 1:4) mediated currents recorded at −20 mV holding potential. Data are shown as mean ± SEM. Each pair of circles represents an individual cell. Scale bars are shown in the figures. The PPR data (pre-cond.) are the same as shown in Figure 2B.

presynaptic expression for all conditions without increased AMPAR/NMDAR ratio, CV analysis yielded a presynaptic locus of expression when the AMPAR/NMDAR ratio increased (compare supplemental information; Table S1). This applies to both 6× 1:1 and 6× 1:4 t-LTP (compare supplemental information, Figures S5 and S6), and is a known erroneous result of CV analysis in case of postsynaptic insertion of new AMPARs at previously silent synapses.[43–47]

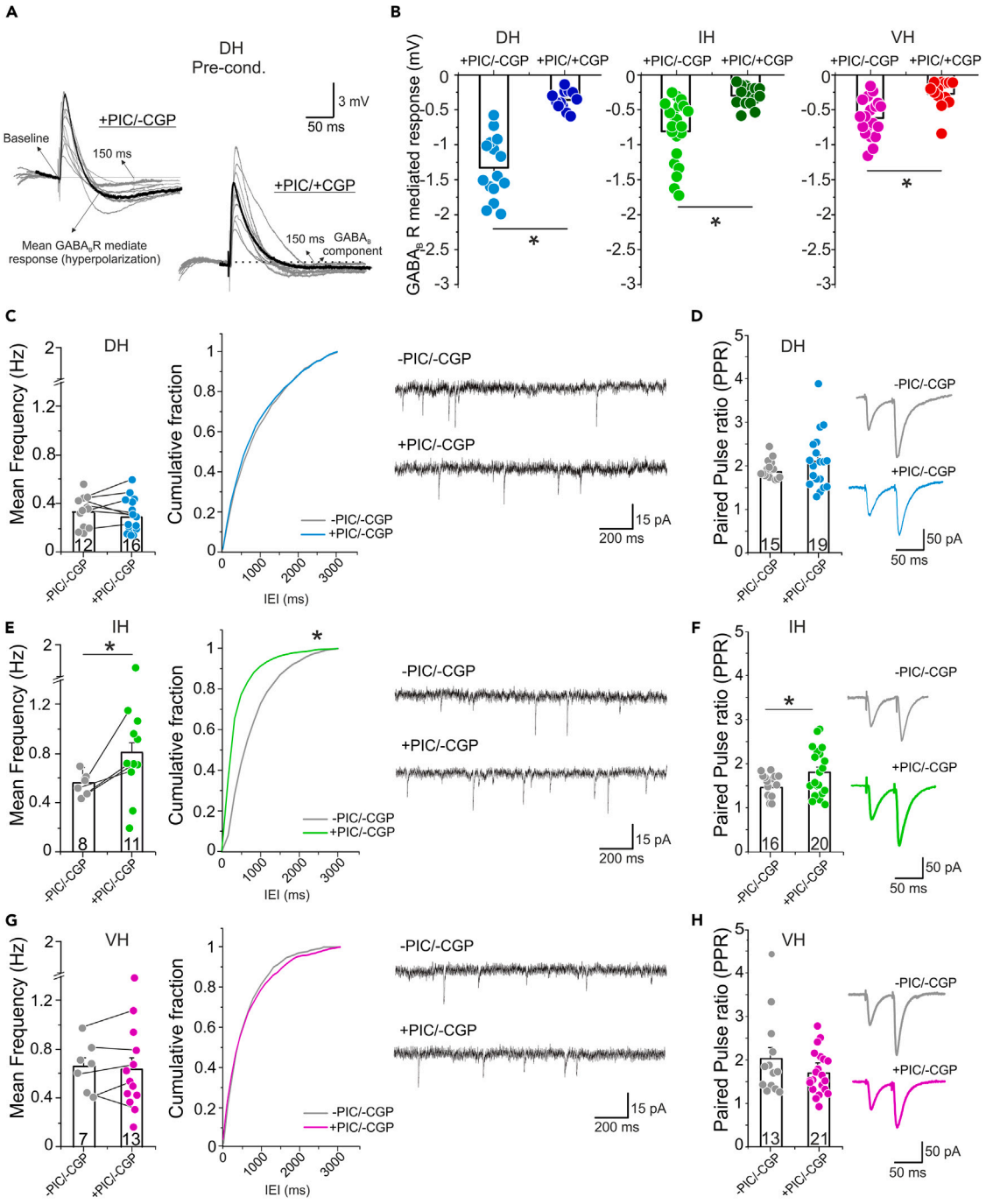

Figure 5. GABAergic inhibition regulates presynaptic glutamate release only in intermediate hippocampus

All recordings were performed in CA1 PCs in VC mode at −70 mV holding potential.

(A) Original traces of EPSPs (depolarization) and delayed GABA$_B$ receptor mediated IPSPs (hyperpolarization) recorded 150 ms after EPSP onset in DH PCs before t-LTP induction, comparing GABA$_B$R mediated responses in the absence (+PIC/-CGP, left) vs. presence of a GABA$_B$R blocker (+PIC/+CGP, right). Single cell traces are shown in gray, averaged responses are represented in black.

(B) SC stimulation induced GABA$_B$R mediated responses in CA1 PCs from DH (+PIC/-CGP: n = 15/N = 8; +PIC/+CGP: n = 12/N = 6), IH (+PIC/-CGP: n = 21/N = 13; +PIC/+CGP: n = 16/N = 9), and VH (+PIC-CGP: n = 19/N = 9; +PIC+CGP: n = 14/N = 10), were significantly reduced in the presence of CGP (GABA$_B$R inhibitor).

(C, E, and G) Mean frequency and cumulative fraction of inter-event intervals (IEI) of putative mEPSCs (see STAR Methods) under conditions of intact GABAergic inhibition (-PIC/-CGP) vs. selective GABA$_A$ receptor blockade (+PIC/-CGP). (C) Picrotoxin did not change pmEPSC frequency in DH

Figure 5. *Continued*

(-PIC/-CGP: n = 12/N = 6; +PIC/-CGP: n = 16/N = 10). (E) Picrotoxin increased pmEPSC frequency in IH (-PIC/-CGP: n = 8/N = 4; +PIC/-CGP: n = 11/N = 8). (G) Picrotoxin did not change pmEPSC frequency in VH (-PIC/-CGP: n = 7/N = 4; +PIC/-CGP: n = 13/N = 8).

(D, F, and H) PPR measurements under conditions of intact GABAergic inhibition vs. selective $GABA_A$ receptor blockade. (D) Picrotoxin did not change PPR in DH (-PIC/-CGP: n = 15/N = 7; +PIC/-CGP: n = 19/N = 9). (F) Picrotoxin increased PPR in IH (-PIC/-CGP: n = 16/N = 9; +PIC/-CGP: n = 20/N = 9). H) Picrotoxin did not change PPR in VH (-PIC/-CGP: n = 13/N = 9; +PIC/-CGP: n = 21/N = 11). Each circle represents an individual cell. The number of recorded cells (n) and animals (N) is indicated in the bars. Data are shown as mean ± SEM. Scale bars are shown in the figures. Paired or unpaired two-tailed t-tests were used and Kolmogorov-Smirnov test for cumulative distribution. (The PPR data under +PIC/-CGP (pre-cond.) are the same as shown in Figure 2B). See also Figure S4.

Overall, these results suggest presynaptic expression of 6× 1:1 t-LTP in VH and IH, while in DH results are consistent with postsynaptic expression. Regarding 6× 1:4 t-LTP, results in all three regions are consistent with a postsynaptic expression mechanism.

Stronger $GABA_B$ receptor mediated inhibition in dorsal than in ventral hippocampus

In the next series of experiments, we wanted to systematically investigate how the two 6× t-LTP paradigms at SC-CA1 synapses depend on $GABA_A$ and $GABA_B$ receptor mediated inhibition along the dorsoventral axis. In the hippocampus, GABA mediates fast inhibitory responses through $GABA_A$ receptors and slow inhibitory responses via $GABA_B$ receptor activity.[48,49] Diverse gradients of $GABA_A$ receptor (DH > IH > VH) and $GABA_B$ receptor (DH < IH < VH) expression were reported along the longitudinal axis of the rat hippocampus.[7] In the previous t-LTP experiments reported here, we always added picrotoxin (100 μM) to block $GABA_A$R responses, while the $GABA_B$R component response that can be inhibited by CGP 55845 (CGP, 10 μM) was intact (+PIC/-CGP condition). To quantify the strength of $GABA_B$ receptor mediated inhibition in our synaptic recordings, we measured the hyperpolarization following the SC stimulation induced EPSPs, which is known to be triggered by SC-dependent activation of GABAergic neurons[50,51] (Figure 5A). Our results obtained in the presence of the $GABA_A$ receptor inhibitor picrotoxin (+PIC/-CGP) revealed stronger $GABA_B$ components in DH compared to VH and IH CA1 neurons (ANOVA $F(2, 52) = 14.71$; $P = <0.0001$, post hoc Tukey-test, $p = 0.135$; DH vs. IH: $p = 0.0007$; DH vs. VH: $P = <0.0001$), being consistent with previous reports.[52,53] To confirm that the observed hyperpolarization was mediated by $GABA_B$ receptors, we added the $GABA_B$R blocker CGP (10 μM) to our picrotoxin containing recording solution (+PIC/+CGP), which strongly inhibited the hyperpolarization (Figure 5A).[54] As represented in Figure 5B, the hyperpolarization after the EPSP in DH reached −1.32 ± 0.11 mV in +PIC/-CGP solution, and was significantly different from the −0.35 ± 0.04 mV recorded in ACSF containing both inhibitors (+PIC/+CGP: unpaired Student's *t* test, $t_{(25)} = 7.37$; $p < 0.0001$). While the $GABA_B$ receptor mediated hyperpolarization was smaller in IH and VH CA1 PCs compared to DH, they were also significantly reduced in the presence of CGP (IH: −0.80 ± 0.1 mV in +PIC/-CGP, and −0.29 ± 0.03 mV in +PIC/+CGP; unpaired Student's *t* test, $t_{(35)} = 4.35$, $p = 0.0001$; VH: −0.6 ± 0.06 mV in +PIC/-CGP, and −0.26 ± 0.05 mV in +PIC/+CGP; unpaired Student's *t* test, $t_{(31)} = 3.908$, $p = 0.0005$; Figure 5B).

Overall, these data suggest that $GABA_B$ receptor mediated inhibition upon SC stimulation reduces excitability of CA1 neurons to a larger extent in DH than in VH.

GABAergic inhibition affects glutamate release probability along the longitudinal axis of the hippocampus

To determine how GABAergic inhibition affects glutamate release at SC-CA1 synapses we compared pmEPSCs recordings with (+PIC/-CGP) and without picrotoxin (-PIC/-CGP; intact physiological GABAergic inhibition), to study effects on glutamate release probability. We found that mean pmEPSC frequencies in DH and VH CA1 PCs were not changed under conditions of intact $GABA_A$R mediated inhibition (DH: +PIC/-CGP: 0.25 ± 0.03 Hz, vs. -PIC/-CGP: 0.31 ± 0.04 Hz; Figure 5C; VH: +PIC/-CGP: 0.63 ± 0.1 Hz, vs. -PIC/-CGP: 0.66 ± 0.07 Hz; Figure 5G), while in IH, intact inhibition via $GABA_A$Rs significantly reduced pmEPSC frequencies (+PIC/-CGP: 0.81 ± 0.01 Hz, vs. -PIC/-CGP: 0.52 ± 0.03 Hz; unpaired Student's *t* test, $t_{(10)} = 2.11$, $p = 0.049$; Figure 5E). Correspondingly, pmEPSC inter-event intervals (IEI) were not affected in both DH and VH under conditions of intact $GABA_A$ receptor mediated inhibition, while in IH IEI intervals were decreased (Kolmogorov–Smirnov two-sample test: $Z = 0.386$, $p < 0.0001$, Figure 5E). Putative mEPSC amplitudes were not affected by picrotoxin in IH (-PIC/-CGP: 13.39 ± 0.12 pA; +-PIC/-CGP: 12.15 ± 0.07 pA) and DH (-PIC/-CGP: 15.87 ± 0.5; +PIC/-CGP: 15.18 ± 0.867), but were significantly increased in VH (-PIC/-CGP: 13.04 ± 0.54; +PIC/-CGP: 15.94 ± 0.54; unpaired Student's T-test, p value = 0.0051; T = 3.362, df = 13).

As a second readout of glutamate release probability, we also determined the PPR at SC-CA1 synapses. While in DH and VH, PPR was not significantly changed by intact $GABA_A$R mediated inhibition (DH: +PIC/-CGP: 2.11 ± 0.14, -PIC/-CGP: 1.86 ± 0.08; Figure 5D, VH: +PIC/-CGP: 1.68 ± 0.1, -PIC/-CGP: 2.02 ± 0.25; Figure 5H), PPR in IH CA1 PCs was significantly reduced under conditions of intact GABAergic conditions compared to $GABA_A$R blockade (+PIC/-CGP: 1.80 ± 0.13, -PIC/-CGP: 1.49 ± 0.07; unpaired Student's *t* test, $t_{(34)} = 2.07$, $p = 0.046$; Figure 5F).

Together, results for PPR and pmEPSC frequencies suggest, that in DH and VH glutamate release probability is not affected by $GABA_A$ receptor blockade, while in IH the results are consistent with changed glutamate release probability in the presence the $GABA_A$ antagonist. This might be explained by tonic inhibition of excitatory neurons by ambient GABA, specifically in IH.

GABAergic inhibition differentially modulates low repeat t-LTP induction at SC-CA1 synapses along the longitudinal axis of the hippocampus

Since our t-LTP results provided clear differences in magnitude and mechanism of expression of t-LTP along the longitudinal axis of the hippocampus (compare Figures 3 and 4), we wanted to investigate how $GABA_A$ and $GABA_B$ receptor mediated inhibition in DH, IH, and VH might account for these differences in t-LTP. Thus, we next compared the efficacy to obtain 6× 1:1 and 6× 1:4 t-LTP along the longitudinal

axis of the hippocampus under conditions of intact GABAergic inhibition (-PIC/-CGP), with t-LTP when only $GABA_A$Rs were inhibited (+PIC/-CGP), or under complete blockade of GABAergic inhibition (+PIC/+CGP).

6× 1:1 t-LTP

Dorsal hippocampus

Our results indicate that in DH the 6× 1:1 t-LTP paradigm failed to induce potentiation under conditions of intact GABAergic (i.e., $GABA_A$ and $GABA_BR$ mediated) inhibition compared to selective $GABA_AR$ blockade or complete GABA receptor blockade (intact inhibition: 95.93 ± 7.0% (n = 9/N = 6), +PIC/-CGP: 180.40 ± 18.03% (n = 9/N = 5), +PIC/+CGP: 190.08 ± 19.02% (n = 6/N = 4); ANOVA $F_{(2,22)} = 5.799$, p = 0.0005, post hoc Tukey-test for intact vs. +PIC/-CGP: p = 0.0014 and for intact inhibition vs. +PIC/+CGP: p = 0.0018; Figure 6A).

Expression mechanism in DH

For DH, we already showed in Figure 4 that successful 6× 1:1 t-LTP did not change the PPR under $GABA_AR$ blockade (+PIC/-CGP, before t-LTP: 2.22 ± 0.24, after t-LTP: 2.16 ± 0.21). Although there was a trend of 6× 1:1 t-LTP under complete blockade of GABAergic responses (+PIC/+CGP) toward reduced PPR (before: 2.80 ± 0.29, after: 2.16 ± 0.19), this effect did not reach statistical significance (paired Student's *t* test, $t_{(5)} = 1.926$, p = 0.11), whereas intact GABAergic inhibition (-PIC/-CGP) blocked 6× 1:1 t-LTP and therefore revealed also no changes in PPR (before: 2.08 ± 0.15, after: 2.12 ± 0.18; Figure 6B left). Similar to 6× 1:1 t-LTP in DH under selective $GABA_AR$ blockade (compare also Figure 4C), we found an increase in AMPAR/NMDAR current ratio also after successful induction of 6× 1:1 t-LTP under complete blockade of GABAergic inhibition (8.93 ± 2.47; Figure 6B right), thus indicating a postsynaptic contribution to t-LTP expression. The CV analysis for both +PIC/-CGP and +PIC/+CGP detects a presynaptic effect for both conditions (supplemental information, Figure S4; Table S1). As mentioned in the context of results shown in Figure 4, this is a known possibly erroneous presynaptic result detected by CV analysis in case of insertion of new AMPA receptors.[43]

Intermediate hippocampus

Interestingly, in the IH region 6× 1:1 t-LTP stimulation induced significant t-LTP when selectively $GABA_AR$s were blocked, compared to complete GABA receptor blockade and intact GABA inhibition (intact: 109.49 ± 13.20% (n = 10/N = 5), +PIC/-CGP: 171.05 ± 12.86% (n = 11/N = 7), and +PIC/+CGP: 122.94 ± 6.10% (n = 9/N = 5); ANOVA $F_{(3,30)} = 14$, p = 0.0009, post hoc Dunn's Test for +PIC/-CGP vs. intact inhibition: p = 0.0013 and for +PIC/-CGP vs. +PIC/+CGP: p = 0.019; Figure 6C). Of note, 6× 1:1 t-LTP stimulation in IH also induced a weak t-LTP under complete GABAergic inhibition compared to non-normalized baseline values (paired Student's *t* test: $t_{(8)} = 4.512$ p = 0.002), therefore indicating significant, but weaker t-LTP.

Expression mechanism in IH

In IH under selective $GABA_AR$ blockade, 6× 1:1 t-LTP was accompanied by decreased PPR (before: 1.86 ± 0.13, after: 1.39 ± 0.08; paired Student's *t* test, $t_{(11)} = 3.719$, p = 0.004; Figure 6D left) and therefore increased glutamate release probability. Since IH showed no 6× 1:1 t-LTP under intact GABAergic conditions (-PIC/-CGP) and only borderline t-LTP under complete blockade of GABAergic inhibition (+PIC/+CGP), the unchanged PPR under both conditions was expected (-PIC/-CGP, before: 1.67 ± 0.08, after: 2.04 ± 0.27; +PIC/+CGP, before: 1.81 ± 0.1, after: 1.68 ± 0.12; Figure 6D left). However, 6× 1:1 stimulation in IH under complete blockade of GABAergic inhibition enhanced the AMPAR/NMDAR current ratio (+PIC/+CGP: 7.52 ± 1.01, +PIC/-CGP: 3.97 ± 0.91; ANOVA $F_{(2,\ 20)} = 3.791$, p = 0.04, post hoc Tukey-test for +PIC/+CGP vs. +PIC/-CGP, p = 0.043; Figure 6D right) although t-LTP was only borderline under these conditions (compare Figure 6C). This might indicate that postsynaptic mechanisms were triggered by this protocol, yet not efficient enough to yield statistically significant 6× 1:1 t-LTP with the ANOVA. This interpretation is corroborated by the absence of a similar increase in AMPAR/NMDAR current ratios under the same +PIC/+CGP conditions in negative controls without t-LTP stimulation (6× 0:0 stimulation: 4.73 ± 0.89). CV analysis yielded presynaptic expression for the 6× 1:1 paradigm under +PIC/-CGP conditions, consistent with the decreased PPR, but allows no clear conclusion for 6× 1:1 in +PIC/+CGP (supplemental information, Figure S4; Table S1).

Ventral hippocampus

In VH, the 6× 1:1 t-LTP paradigm induced significant potentiation regardless of GABAergic inhibition in all three conditions (intact: 138.72 ± 12.76% (n = 8/N = 5), +PIC/-CGP: 135.93 ± 6.61% (n = 12/N = 9), +PIC/+CGP: 143.35 ± 12.40% (n = 8/N = 6); Figure 6E).

Expression mechanism in VH

In VH, successful 6× 1:1 t-LTP did neither affect PPR under intact GABAergic conditions (-PIC/-CGP, before: 1.93 ± 0.29, after: 1.64 ± 0.17), nor under complete GABA receptor blockade (+PIC/+CGP, before: 1.93 ± 0.11, after: 1.92 ± 0.22), but significantly reduced PPR under selective $GABA_AR$ blockade (+PIC/-CGP, before: 1.82 ± 0.2, after: 1.30 ± 0.09; paired Student's *t* test, $t_{(10)} = 3.719$, p = 0.004; Figure 6F right). This is consistent with presynaptic expression of 6× 1:1 t-LTP under +PIC/-CGP conditions, but seems to indicate that 6× 1:1 t-LTP expression under intact GABAergic inhibition and under complete blockade of GABAergic inhibition cannot be clearly assigned to presynaptic mechanisms. Regarding postsynaptic expression mechanisms after successful 6× 1:1 t-LTP induction, no significant increase in AMPAR/NMDAR current ratio was observed, neither under conditions of selective $GABA_AR$ blockade (4.75 ± 0.91), intact GABAergic inhibition (4.87 ± 1.14), or

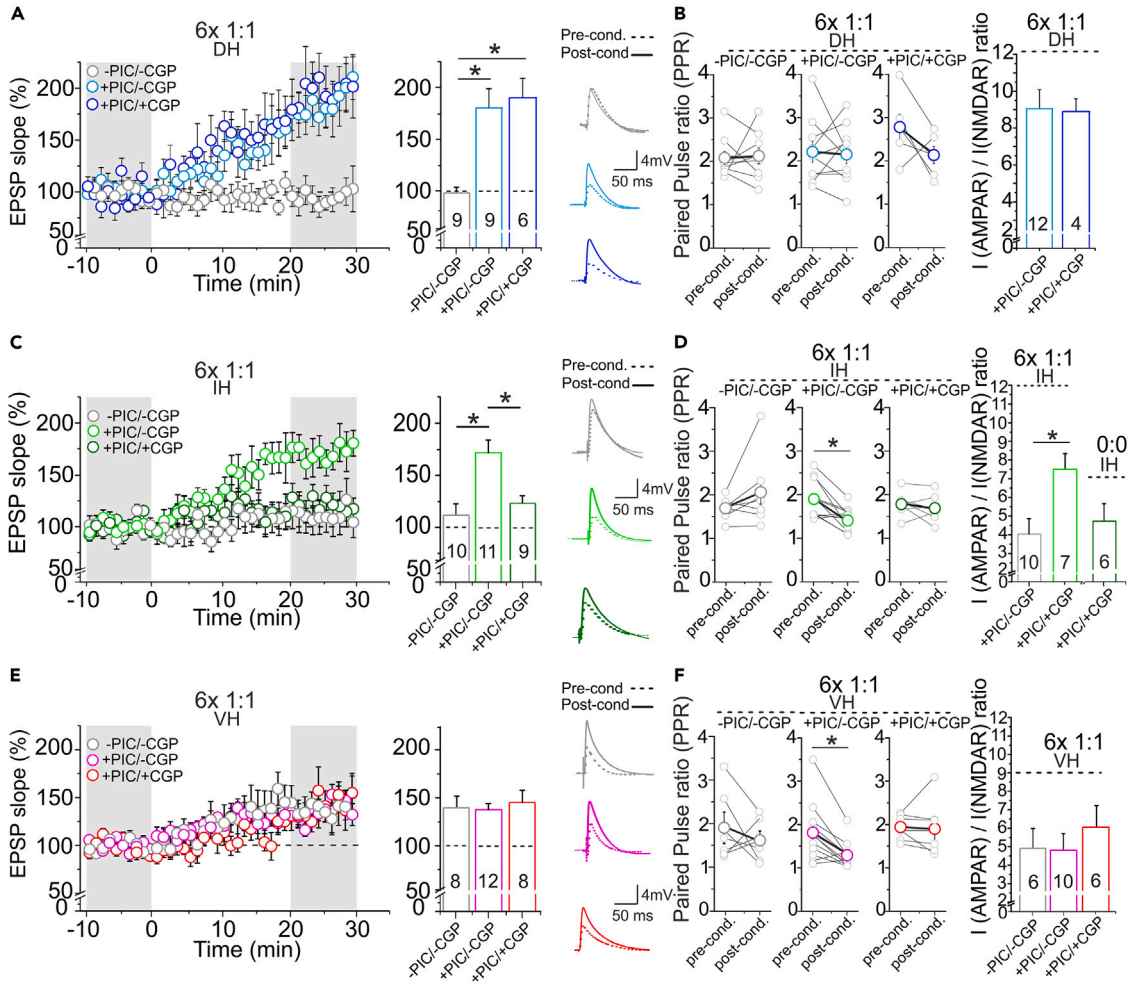

Figure 6. GABAergic modulation of low repeat 1:1 t-LTP magnitude along the longitudinal axis of the hippocampus

(A) 6× 1:1 t-LTP in CA1 PCs of DH under intact GABAergic inhibition (-PIC/-CGP: n = 9/N = 6), in response to selective $GABA_AR$ inhibition (+PIC/-CGP: n = 9/N = 5), and upon complete blockade of GABAergic inhibition (+PIC/+CGP: n = 6/N = 4). 6× 1:1 t-LTP was absent under intact GABAergic inhibition.

(B) Paired pulse ratio (PPR) pre-vs. post-conditioning in PCs of DH under intact GABAergic inhibition (-PIC/-CGP: n = 9/N = 6), $GABA_AR$ blockade (+PIC/-CGP: n = 10/N = 7), and upon complete blockade of GABAergic inhibition (+PIC/+CGP: n = 5/N = 5) shows no significant changes. Increased (compared to negative control in Figure 4C; 0:0 protocol) AMPAR/NMDAR current ratio suggests that 6× 1:1 t-LTP under selective $GABA_AR$ blockade (n = 12/N = 7) and under complete blockade of GABAergic inhibition (n = 4/N = 4) is expressed post-synaptically.

(C) 6× 1:1 protocol in PCs of IH under intact GABAergic inhibition (n = 10/N = 5), upon selective $GABA_AR$ inhibition (n = 11/N = 7), and upon complete blockade of GABAergic inhibition (n = 9/N = 5). Significant 6× 1:1 t-LTP was only induced upon selective blockade of $GABA_A$ receptor inhibition.

(D) Successful 6× 1:1 t-LTP in IH upon selective $GABA_AR$ blockade (n = 12/N = 8) significantly reduced PPR suggesting presynaptic t-LTP expression. PPR was unaffected in the absence of 6× 1:1 t-LTP observed under intact GABAergic inhibition (n = 8/N = 7), and under complete blockade of GABAergic inhibition (n = 7/N = 6). Increased AMPAR/NMDAR current ratio under conditions of complete blockade of GABAergic inhibition indicates postsynaptic changes after 6× 1:1 t-LTP (n = 7/N = 6). AMPAR/NMDAR current ratio was not changed upon selective $GABA_AR$ blockade (n = 10/N = 6), and was also unchanged under non-stimulated negative control condition (0:0 protocol; n = 6/N = 3).

(E) Successful 6× 1:1 t-LTP in CA1 PCs of VH under intact GABAergic inhibition (-PIC/-CGP: n = 8/N = 5), in response to selective $GABA_AR$ inhibition (+PIC/-CGP: n = 12/N = 9), and upon complete blockade of GABAergic inhibition (+PIC/+CGP: n = 8/N = 6).

(F) Despite successful 6× 1:1 t-LTP in PCs of VH independent of GABAergic inhibition, PPR pre-vs. post-conditioning was significantly reduced only under selective $GABA_AR$ blockade (n = 11/N = 7), but remained unaffected under intact GABAergic inhibition (n = 7/N = 5), and under complete blockade of GABAergic inhibition (n = 7/N = 5). Irrespective of GABAergic conditions, AMPAR/NMDAR current ratio remained unchanged following successful induction of 6× 1:1 t-LTP (n = 6/N = 4 for intact inhibition (n = 6/N = 5 for complete block of GABA inhibition; n = 10/N = 5 for selective $GABA_AR$ blockade). Time course of t-LTP during 30 min of recording after t-LTP induction is represented on the left side of each panel. Original traces of EPSPs before and after t-LTP induction under diverse GABAergic inhibition are shown on the right. The number of recorded cells (n) and animals (N) is indicated in the bars. Data are shown as mean ± SEM. Multiple comparisons were performed with ANOVA using post hoc Tukey's test. (For better direct comparison, some of the PPR data shown in B, D, F are the same as shown in Figure 4B). See also Figure S5.

complete blockade of GABAergic inhibition (6.05 ± 1.13; Figure 6F left). These non-conclusive results for expression mechanism of 6× 1:1 t-LTP in VH might result from the low magnitude of t-LTP observed under these conditions. Results of CV analysis are consistent with presynaptic expression under -PIC/-CGP and +PIC/-CGP conditions, but postsynaptic expression under complete block of GABAergic inhibition (supplemental information, Figure S5; Table S1).

6× 1:4 t-LTP

Dorsal hippocampus

In the next step, we performed the same set of experiments with GABA receptor inhibitors for the 6× 1:4 (burst) protocol (Figure 7). We found that at the DH pole, the 6× 1:4 t-LTP protocol induced similar magnitudes of potentiation in all three conditions (intact GABAergic inhibition: 139.51 ± 15.74% (n = 6/N = 4), +PIC/-CGP: 179.75 ± 15.53% (n = 8/N = 4), complete blockade of GABAergic inhibition: 150.20 ± 16.60% (n = 6/N = 5); Figure 7A).

Expression mechanism in DH

In DH, successful 6× 1:4 t-LTP did neither affect PPR under intact GABAergic conditions (-PIC/-CGP, before: 2.06 ± 0.2, after: 2.25 ± 0.35), nor under complete GABA receptor blockade (+PIC/+CGP, before: 2.41 ± 0.2, after: 2.06 ± 0.16; Figure 7B left), speaking against presynaptic t-LTP expression. Successful 6× 1:4 t-LTP in DH under selective $GABA_AR$ blockade showed an increased AMPAR/NMDAR current ratio (+PIC/-CGP: 9.15 ± 1.19), speaking in favor of postsynaptic expression of t-LTP. However, under intact GABAergic inhibition (-PIC/-CGP: 2.66 ± 0.41) or complete blockade of GABAergic inhibition (+PIC/+CGP: 3.68 ± 0.52) 6× 1:4 t-LTP was most likely not mediated by postsynaptic increase in AMPAR conductance. Accordingly, we found a significantly increased AMPAR/NMDAR current ratio between selective $GABA_AR$ blockade and intact GABAergic inhibition (Kruskal–Wallis test $H_{(3)} = 14.15$, $p < 0.0008$; Figure 7B right). This points toward an altered (i.e., not clearly pre- or postsynaptic) expression mechanism for 6× 1:4 t-LTP when GABAergic inhibition is either fully functional or fully blocked. CV analysis (supplemental information, Figure S5; Table S1) revealed a clear presynaptic mechanism for +PIC/-CGP and +PIC/+CGP conditions, and a postsynaptic mechanism for fully functional inhibition.

Intermediate hippocampus

The 6× 1:4 t-LTP paradigm induced clear potentiation under intact GABAergic inhibition and in the presence of only the $GABA_A$ receptor inhibition (intact: 164.38 ± 20.82% (n = 10/N = 5), +PIC/-CGP: 149.02 ± 19.67% (n = 11/N = 5), whereas there was no t-LTP under complete GABA receptor blockade (+PIC/+CGP: 107.60 ± 5.31% (n = 11/N = 7); Paired Student's *t* test, t(9) = 0.736 p = 0.48; Figure 7C).

Expression mechanism in IH

In IH, PPR was significantly reduced under intact GABAergic inhibition (-PIC/-CGP, before: 1.68 ± 0.12, after: 1.46 ± 0.09; paired Student's *t* test, $t_{(9)} = 3.569$, p = 0.006; Figure 7D left), being consistent with presynaptic expression. PPR remained unchanged under complete blockade of GABAergic inhibition (+PIC/+CGP, before: 1.73 ± 0.11, after: 1.74 ± 0.07), which is consistent with absence of 6× 1:4 t-LTP under these conditions. While successful 6× 1:4 t-LTP in IH under conditions of selective $GABA_AR$ blockade significantly increased the AMPAR/NMDAR current ratio (+PIC/-CGP: 9.77 ± 1.28), thus suggesting postsynaptic expression of t-LTP, the absence of 6× 1:4 t-LTP under complete blockade of GABAergic inhibition (+PIC/+CGP) did – as expected – also not reveal a change in the AMPAR/NMDAR current ratio (5.59 ± 1.14). Unexpectedly, successful 6× 1:4 t-LTP in IH under intact GABAergic conditions (-PIC/-CGP) was not accompanied by a change in the AMPAR/NMDAR current ratio (5.16 ± 0.63). ANOVA analysis of AMPAR/NMDAR current ratio revealed significant differences between selective $GABA_A$ receptor blockade and the two other conditions (i.e., +PIC/+CGP and -PIC/-CGP: $F_{(2, 25)} = 4.823$ p = 0.0169, post hoc Tukey-test for +PIC/-CGP vs. PIC/-CGP p = 0.036, and +PIC/-CGP vs. complete GABA blockade: p = 0.05; Figure 7D right). This might indicate that 6× 1:4 t-LTP under -PIC/-CGP conditions does not show the same postsynaptic changes as observed under selective $GABA_AR$ blockade. CV analysis (Figure S6; Table S1) is consistent with a presynaptic mechanism for +PIC/-CGP but does not allow to draw a clear conclusion for intact GABAergic conditions.

Ventral hippocampus

ANOVA statistical analysis yielded a similar pattern of t-LTP for 6× 1:4 t-LTP in PCs of VH in all studied conditions as in IH (intact: 139.60 ± 12.03% (n = 9/N = 5), +PIC/-CGP: 137.80 ± 11.01% (n = 10/N = 7), complete blockade: 106.45 ± 10.55% (n = 8/N = 5); ANOVA $F_{(2, 24)} = 2.548$, p = 0.099; Figure 7E). Both intact and +PIC/-CGP conditions revealed significant t-LTP compared to 100% baseline (one sample t-test p = 0.011, and p = 0.007, respectively). However, 6× 1:4 t-LTP failed to induce significant t-LTP at SC-CA1 synapses in VH under complete GABA receptor blockade (one-sample t-test p = 0.56; Figure 7E).

Expression mechanism in VH

Similar to observations for IH, 6× 1:4 t-LTP in VH was accompanied by decreased PPR (-PIC/-CGP, before: 1.70 ± 0.14, after: 1.46 ± 0.1; paired Student's *t* test, $t_{(7)} = 2.372$, p = 0.049; Figure 7F left), whereas under complete blockade of GABAergic inhibition (+PIC/+CGP), PPR remained unaffected (before: 2.00 ± 0.24, after: 1.85 ± 0.15). Likewise, also in VH AMPAR/NMDAR current ratio after successful 6× 1:4 t-LTP was significantly enhanced under selective $GABA_AR$ blockade (+PIC/-CGP: 10.13 ± 0.72) but not after successful t-LTP under conditions of intact GABAergic inhibition (-PIC/-CGP: 5.86 ± 0.33).

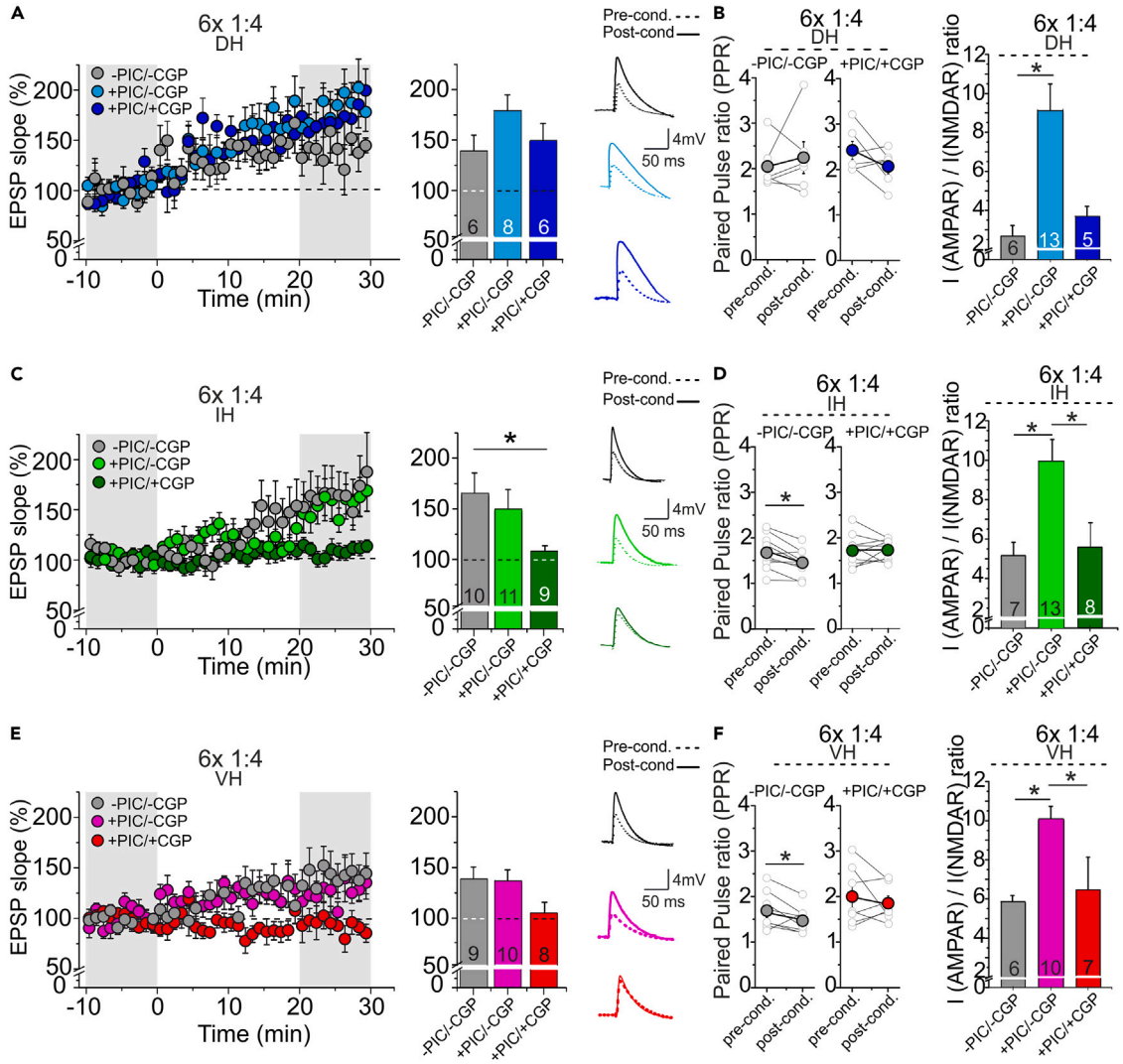

Figure 7. GABAergic modulation of low repeat 1:4 t-LTP magnitude at hippocampal SC-CA1 synapses along the longitudinal axis

(A) 6× 1:4 protocol in DH region induced t-LTP independent of GABAergic modulation under intact conditions (-PIC/-CGP: n = 6/N = 4), upon selective $GABA_AR$ blockade (+PIC/-CGP: n = 8/N = 4), or upon complete blockade GABAergic inhibition (+PIC/+CGP: n = 6/N = 5).

(B) Paired pulse ratio (PPR) pre-vs. post-conditioning in DH PCs under intact GABAergic inhibition (-PIC/-CGP: n = 6/N = 4), and upon complete blockade of GABAergic inhibition (+PIC/+CGP: n = 6/N = 5) showed no significant changes. The AMPAR/NMDAR current ratio in DH was increased following successful 6× 1:4 t-LTP only under selective $GABA_AR$ blockade (n = 13/N = 8), while AMPAR/NMDAR current ratio was unaffected after 6× 1:4 t-LTP under intact GABAergic inhibition (n = 6/N = 4) and under complete blockade of GABAergic inhibition (n = 5/N = 4).

(C) In IH, 6× 1:4 stimulation induced strong t-LTP under intact GABAergic inhibition (-PIC/-CGP: n = 10/N = 5) and no significant potentiation under complete blockade of GABAergic inhibition (+PIC/+CGP: n = 9/N = 5). Under selective $GABA_AR$ inhibition (+PIC/-CGP: n = 11/N = 7), 6× 1:4 t-LTP showed an intermediate t-LTP magnitude.

(D) PPR pre-vs. post-conditioning was reduced in IH after successful induction of t-LTP under intact GABAergic inhibition (-PIC/-CGP: n = 10/N = 5), but not in the absence of t-LTP under complete blockade of GABAergic inhibition (+PIC/+CGP: n = 10/N = 4). 6× 1:4 t-LTP induction in IH enhanced AMPAR/NMDAR current ratio under $GABA_AR$ blockade (n = 13/N = 9) compared to intact GABAergic inhibition (n = 7/N = 5), and complete blockade of GABAergic inhibition (n = 8/N = 5).

(E) Similar to IH 6× 1:4 t-LTP in VH was successfully induced, under conditions of intact GABAergic inhibition (-PIC/-CGP: n = 9/N = 5), upon selective $GABA_AR$ inhibition (+PIC/-CGP: n = 10/N = 7), but not upon complete blockade of GABAergic inhibition (+PIC/+CGP: n = 8/N = 5).

(F) PPR pre-vs. post-conditioning in VH was reduced after successful induction of t-LTP under intact GABAergic inhibition (-PIC/-CGP: n = 8/N = 4), but unchanged in the absence of t-LTP under complete blockade of GABAergic inhibition (+PIC/+CGP: n = 7/N = 4). AMPAR/NMDAR current ratio was only increased after successful induction of 6× 1:4 t-LTP under selective $GABA_AR$ blockade (n = 10/N = 7), but was despite successful t-LTP unaffected under intact GABAergic inhibition (n = 6/N = 5), and in the absence of t-LTP under complete blockade of GABAergic inhibition (n = 7/N = 5). The number of recorded cells (n) and animals (N) is indicated in the bars. Data are shown as mean ± SEM. Multiple comparisons were performed with ANOVA using post hoc Tukey's test. (For better direct comparison, some of the PPR data shown in B, D, F are the same as shown in Figure 4B). See also Figure S6.

As expected, absence of 6× 1:4 t-LTP under complete blockade of GABAergic inhibition was also not accompanied by increased AMPAR/NMDAR current ratios (+PIC/+CGP: 6.45 ± 1.70; ANOVA $F_{(2, 20)} = 5.421$, $p = 0.0127$, post hoc Tukey-test for +PIC/-CGP vs. intact $p = 0.024$, and +PIC/-CGP vs. complete blockade $p = 0.044$; Figure 7F right). Thus, while these results for AMPAR/NMDAR current ratios are consistent with postsynaptic expression of 6× 1:4 t-LTP under selective $GABA_AR$ blockade, the same protocol does not reveal postsynaptic expression under conditions of intact GABAergic inhibition, but shifts to presynaptic expression in both IH and VH regions. The CV analysis (Figure S6; Table S1) detected a presynaptic mechanism for +PIC/-CGP conditions. As mentioned before, this is a known possibly erroneous presynaptic result detected by CV analysis in case of insertion of new AMPA receptors.[43] For 6× 1:4 t-LTP under intact GABAergic conditions, CV analysis cannot clearly distinguish between pre- and postsynaptic mechanisms.

Together, these results suggest a complex regulation of 6× 1:1 and 6× 1:4 t-LTP by $GABA_A$ and $GABA_B$ receptor mediated mechanisms that are co-activated in the SC-CA1 circuit by our extracellular SC stimulation. Importantly, these GABAergic mechanisms, which control t-LTP, are differentially recruited along the longitudinal axis of the hippocampus. Blockade of only $GABA_A$ receptor mediated transmission allowed successful induction of 6× 1:1 t-LTP in DH, IH, and VH. Under intact GABAergic conditions, 6× 1:1 t-LTP could be induced only in VH, while intact $GABA_BR$ mediated inhibition was beneficial for successful induction of 6× 1:1 t-LTP selectively in IH (compare Figure 6).

In stark contrast, 6× 1:4 t-LTP was successfully induced in all three areas under conditions of intact GABAergic inhibition (-PIC/-CGP) and if only $GABA_A$ receptors were blocked (+PIC/-CGP). However, complete blockade of $GABA_A$ and $GABA_B$ receptor mediated mechanisms, abolished 6× 1:4 t-LTP in IH and VH (compare Figure 7).

One could argue that the absence of t-LTP under conditions of complete blockade of GABAergic inhibition is due to spontaneous potentiation (i.e., elevated baseline excitation), thereby saturating the LTP machinery. However, this should lead to systematically increased EPSP amplitudes or reduced stimulation strength required to induce half-maximal EPSP amplitudes in +PIC/+CGP. However, this was not observed in our recordings (compare Figure S4).

Overall, these results (summarized in supplemental information: Table S1) indicate a diverse set of expression mechanisms for 6× 1:1 and 6× 1:4 t-LTP along the longitudinal axis of the hippocampus that crucially depend on conditions for GABAergic transmission, stressing the important role of feedforward and feedback inhibition in regulating SC-CA1 synaptic plasticity. For better explanation of the complex interactions leading to these different types of t-LTP expression in IH, we provide schemes in the supplemental information (compare Figures S8 and S9).

DISCUSSION

Our patch clamp recordings in mouse hippocampal slices revealed gradients of CA1 PC properties along the dorsoventral axis. The two low repeat t-LTP paradigms (6× 1:1 and 6× 1:4) induced robust t-LTP in all regions, albeit with a gradient of t-LTP magnitudes from ventral to dorsal pole (VH < IH < DH). The expression mechanisms of both t-LTP versions vary along the dorsoventral axis and depend on subtle regulation by $GABA_A$ and $GABA_B$ receptor mediated inhibition.

Taken together, these results suggest an intricate regulation of low repeat t-LTP at SC-CA1 synapses along the dorsoventral axis.

We discuss our data in relation to previous results that were, however, mainly recorded in rat hippocampus.

Differences in intrinsic excitability and basal synaptic properties of CA1 neurons along the longitudinal axis of the hippocampus

We observed a more depolarized RMP and higher firing frequencies in VH/IH compared to DH. (Figures 1B and 1C). Both properties indicate a stronger intrinsic excitability of CA1 cells in VH/IH, which is consistent with previous results in rat hippocampus.[6] In comparison to this study, we also included recordings in the intermediate region (IH), and found that basal properties of IH and VH are very similar. Other studies also described electrophysiologically distinct subpopulations of CA1 PCs along the transversal and the radial axis of the hippocampus being in line with increasing excitability from DH to VH.[55,56] Changes in neuronal morphology can affect ionic conductance and somatic input resistance (R_{in}) of neurons, and were used to explain the distinct intrinsic excitability in rat DH CA1 PCs.[6] A larger dendritic surface in DH CA1 neurons can reduce R_{in}, being consistent with the increased rheobase of DH PCs in our mouse recordings (Figure S1). Higher excitability of our mouse VH PCs might originate from an increased ratio of excitatory to inhibitory synaptic inputs to VH CA1 neurons, as suggested for rats.[53,57] In accordance with these previous data in rats, our synaptic I/O curves clearly indicate a steep increase of excitatory drive at SC inputs from DH to VH (compare Figure 1), being consistent with distinct expression patterns of ligand- and voltage-gated ion channels in VH vs. DH in rats.[36,55,58–60] Together, these properties seem to account for the higher excitability of postsynaptic CA1 neurons and the steeper slope in excitatory synaptic I/O curves in ventral CA1 (compare Figure 1E and Daoudal, 2003).[61]

Regarding glutamate release at SC-CA1 synapses, we observed significantly weaker PPF in VH compared to DH. These data speak in favor of higher initial release probability in VH, being consistent with results in rat hippocampus.[53] At the network level, GABA-mediated recurrent inhibition (RI) was described to control CA1 excitatory output in VH less efficiently than in DH.[52] Importantly, both GABA and glutamate release are also affected by neuromodulator releasing (i.e., noradrenergic and dopaminergic inputs) axonal projections to the hippocampus, which are more prominent in VH than DH.[3] VTA neurons prominently project dopaminergic fibers to VH, but not to DH, and locus coeruleus (LC) noradrenergic terminals show 40% higher density in VH vs. DH.[62] Both neuromodulators can therefore enhance cellular excitability through second-messenger mediated biochemical changes.[63] On the postsynaptic side of SC-CA1 synapses, previous studies showed distinct NMDAR subunit composition along the dorsoventral axis. Thus, a lower NR2A/NR2B ratio was detected in VH than in DH, leading to a weaker magnesium block and slower decay of NMDAR mediated EPSP components in VH.[6,64] Together, these differences affect AMPAR and NMDAR components of EPSPs. The EPSC decay time constants are mainly regulated by NMDAR activation and deactivation,

and the NR2A/NR2B ratio, and the more prolonged EPSC decay that we observed in VH compared to DH (compare Figure S2) is in line with similar results reported for rat hippocampus.[6]

Magnitude of timing-dependent LTP induced by 6× 1:1 and 6× 1:4 paradigms along the longitudinal axis of the hippocampus

We previously introduced two low repeat STDP paradigms, which induce robust t-LTP in IH.[31] In the present study, we now investigated differences in magnitude and mechanisms involved in low repeat t-LTP induction and expression along the longitudinal axis of the hippocampus. In the presence of picrotoxin (+PIC/-CGP) both STDP paradigms revealed significant potentiation in all three hippocampal CA1 regions along the dorsoventral axis (Figure S3), still the magnitude of 6× 1:1 t-LTP in DH PCs was significantly higher compared to the VH (Figure 3E). Several mechanisms possibly underlie these differences. First, the described higher release probability and steeper I/O curves for basal SC-CA1 synaptic transmission in VH compared to DH (compare Figure 1) might indicate that there is less capacity for further increase in synaptic plasticity in VH. Secondly, Sholl analysis[65] indicated that CA1 PCs in VH possess fewer dendritic branches and less dendritic surface area than DH,[66] providing less dendritic space for activity-dependent formation of new synaptic contacts. Moreover, the differences in dendritic structure, in conjunction with distinct profiles of voltage-dependent dendritic ion channels[67] between DH and VH could lead to distinct efficacy of AP backpropagation to postsynaptic sites, thereby affecting postsynaptic Ca^{2+} elevations required for inducing t-LTP. Here, we previously reported that successful induction of 6× 1:1 t-LTP depends on Ca^{2+} influx through NMDARs and VGCCs to induce synaptic changes.[31] Interestingly, it was shown in rat hippocampus that VGCCs interact more effectively with NMDARs in DH than in the VH,[68] which would be consistent with stronger t-LTP in DH vs. VH.

At the network level, weaker GABAergic inhibition was reported in VH than in DH,[53] but since we initially induced × 1:1 t-LTP paradigms in the presence of the $GABA_A$R inhibitor picrotoxin (Figure 3), GABAergic effects can most probably not account for stronger 6× 1:1 t-LTP in DH under these recording conditions. Of note, when trying to compare 6× 1:1 t-LTP magnitudes along the dorsoventral axis it has to be kept in mind that expression mechanisms differ. While the 6× 1:1 t-LTP in IH and VH (Figure 4) is expressed presynaptically, 6× 1:1 t-LTP in DH PCs appears to be expressed by postsynaptic insertion of new AMPARs (compare Table S1). Thus, more effective 6× 1:1 t-LTP in DH might be explained by switching from pre-to postsynaptic expression between VH and DH.

Efficacy of 6× 1:4 t-LTP in the presence of picrotoxin (+PIC/-CGP) shows a gradient along the dorsoventral axis (DH > VH), but this effect does not reach statistical significance. In case of 6× 1:4 t-LTP, there is also no change in the t-LTP expression mechanism along the dorsoventral axis, with DH, IH, and VH all depending on AMPAR insertion into the postsynaptic membrane (compare Figures 4C; Table S1). Under baseline conditions, we observed a slightly lower AMPAR/NMDAR ratio in DH than in IH and VH (Figure 4C), which could indicate a stronger contribution of NMDAR or VGCC mediated Ca^{2+} influx during induction of 6× 1:4 t-LTP in DH. Since previous studies in rats indicated either higher or lower expression of AMPARs in VH vs. DH[36] and[69] it remains unclear whether distinct ratios of AMPAR/NMDAR along the dorsoventral axis might explain the slight difference in 6× 1:4 t-LTP magnitude. Nevertheless, the changes in AMPAR/NMDAR ratio after 6× 1:4 t-LTP in all hippocampal subfields indicate a similar level of new AMPAR insertion.

GABAergic modulation of 6× 1:1 t-LTP induction along the longitudinal axis of the hippocampus

GABAergic inhibition regulates the activity and balance of neuronal responses during excitation and modulates release of neuromodulators.[70–72] In all previous experiments, we blocked $GABA_A$ receptors with 100 μM picrotoxin. In the next step, we recorded 6× 1:1 and 6× 1:4 t-LTP under conditions of intact GABAergic inhibition, allowing to evaluate the role of $GABA_A$R signaling in the induction of t-LTP. A previous study suggested opposite gradients of $GABA_A$R (DH > IH > VH) and $GABA_B$R expression (DH < IH < VH) along the longitudinal axis in rat hippocampus.[7] However, we found a higher $GABA_B$R mediated component response in DH than in IH and VH (Figures 5A and 5B) in mouse slices. These seemingly discordant results could indicate a species difference or might reflect that receptor activation is not only a function of receptor expression but also of GABA release, which might differ between DH and VH CA1 circuits. Yet, no previous study reported differences in extracellular GABA levels along the dorsoventral axis. Regarding its role in t-LTP, GABA is known to act as a Hebbian/anti-Hebbian switch, which mainly acts on postsynaptic $GABA_A$ receptors of CA1 PCs.[73] At the same time, GABAergic modulation at presynaptic glutamatergic terminals is even more complex. Thus, at hippocampal mossy fiber synapses it was reported that $GABA_A$R activation can depolarize presynaptic terminals.[74,75] However, controversial results exist whether this depolarization reduces[76,77] or rather enhances glutamate release.[78,79] While all these previous results were obtained by exogenous application of the $GABA_A$R agonist muscimol to measure changes in glutamate release, we here addressed physiological activation of $GABA_A$Rs. Muscimol application in acute hippocampal slices reduced axonal excitability.[74] This is consistent with lower glutamate release under intact GABAergic inhibition (-PIC/-CGP) compared to selective $GABA_A$R blockade (+PIC/-CGP) observed here. Our pmEPSC recordings (Figure 5), revealed significantly increased glutamate release probability only in IH, when $GABA_A$ receptors were inhibited (+picrotoxin). The intermittent location of IH along the dorsoventral axis, where both glutamate release probability (DH < IH < VH, Figure 2), and GABAergic inhibition as well as $GABA_A$R expression (DH > IH > VH) are in balance might provide a specific control over glutamate release.[7] Moreover, GABAergic signaling also controls dopamine release from dopaminergic fibers,[70] thereby modulating excitability of pre- and postsynaptic cells of glutamatergic synapses through regulation of voltage-gated ion channels.[80,81] This complex interaction of GABAergic and dopaminergic regulation could account for our observation that glutamate release probability at SC-CA1 synapses in IH is increased under conditions of intact GABAergic inhibition (Figure 5).

6× 1:1 t-LTP in VH was unaffected under intact GABAergic inhibition, possibly due to higher basal presynaptic glutamate release probability compared to IH region (Figure 2), as was suggested previously for rat hippocampus.[34,82] Moreover, the reported weaker GABAergic

inhibition in VH of rats,[53] could render 6× 1:1 t-LTP less sensitive for GABAergic modulation also in mice. This was confirmed by our observation that in VH 6× 1:1 t-LTP was merely insensitive to both $GABA_A$ and $GABA_B$ receptor mediated inhibition. On the same vein, the glutamate release profile in VH remained unaffected by $GABA_A$R activation (Figure 5). These results suggest that 6× 1:1 t-LTP in the VH is largely independent from GABAergic inhibition.

In DH, 6× 1:1 t-LTP is expressed post-synaptically and glutamate release is not affected by GABAergic inhibition. At the postsynaptic site, intact GABAergic inhibition (-PIC/-CGP) reduces CA1 PC excitability, thereby suppressing activation of L-type-VGCC and NMDARs, which are critical for induction of 6× 1:1 t-LTP.[31] This might explain the absence of 6× 1:1 t-LTP in DH when GABAergic inhibition is intact.

Several studies suggest that[83–85] that modulation and expression of different types of synaptic plasticity crucially depend on $GABA_A$Rs trafficking.[86] Yet, the role of $GABA_B$Rs in regulating t-LTP – is largely unknown. At the presynaptic site, $GABA_B$R blockade seems to enhance glutamate release probability,[87] which would be expected to facilitate 6× 1:1 t-LTP in IH and VH. However, complete blockade of GABAergic inhibition (+PIC/+CGP) did not affect 6× 1:1 t-LTP in VH (and even blocked 6× 1:1 t-LTP in IH (Figure 6). Several *in vivo* and *in vitro* studies on rat slices revealed a complex modulation of LTP by $GABA_B$R signaling, and the type of stimulation appeared to influence the effect of $GABA_B$R mediated inhibition for LTP outcome While one group found that blocking $GABA_B$Rs facilitates LTP in CA1 of rats,[88] opposing results were reported by others.[89] Importantly, a study in dentate gyrus of rat hippocampal slices revealed that NMDAR-dependent LTP is critically dependent on the reduction of inhibition (disinhibition) provided by $GABA_B$R activation.[90] This disinhibition in rat hippocampal slices is mainly provided by GABA mediated reduction of GABA release via $GABA_B$ autoreceptors on GABAergic terminals.[91] As we previously reported that 6× 1:1 t-LTP in IH is NMDAR-dependent,[31] a similar mechanism of $GABA_B$R mediated disinhibition of presynaptic glutamate release could account for our observation of blocked 6× 1:1 t-LTP under complete blockade of GABAergic inhibition in IH (Figures 6C and S8). In DH, 6× 1:1 t-LTP induction occurred independent from NMDAR activation (Figure S10). Thus, $GABA_B$R mediated disinhibition of CA1 PCs might not be required for LTP in DH, explaining the robust 6× 1:1 t-LTP observed under conditions of complete blockade of GABAergic inhibition (Figure 6A).

GABAergic modulation of 6× 1:4 t-LTP induction along the longitudinal axis of the hippocampus

While our 6× 1:4 t-LTP paradigm induced robust t-LTP in DH independent of GABAergic inhibition, the magnitude of t-LTP in IH and VH was not affected by $GABA_A$ receptor blockade but highly sensitive to additional $GABA_B$ receptor antagonism (compare Figure 7). Two types of glutamatergic inputs control GABA release from interneurons: SC stimulation leads to feedforward inhibition, while feedback inhibition is triggered by postsynaptic spiking of CA1 PCs.[92,93] Burst stimulation of postsynaptic CA1 neurons, as we induce with our 6× 1:4 paradigm, could activate stronger feedback-inhibition, increasing GABA release, which then activates $GABA_B$ autoreceptors on presynaptic terminals of interneurons, potently suppressing further GABA release, thereby causing disinhibition of CA1 neurons.[91,94] In this way, burst stimulation with 6× 1:4 stimulation under intact GABAergic inhibition could lower GABA release at inhibitory synapses not only onto CA1 neurons but also onto dopaminergic fibers, thus stimulating DA release, which is essential for induction of 6× 1:4 t-LTP.[31] Lower levels of GABAergic inhibition onto CA1 PCs through $GABA_B$ autoreceptors on GABAergic terminals will thus facilitate CA1 cell depolarization, allowing to induce robust t-LTP in all studied hippocampal regions (Figures 7 and S9). Minor differences in magnitudes of 6× 1:4 t-LTP seen with intact GABAergic inhibition might result from differences in the efficacy of $GABA_A$ receptor mediated inhibition (DH > IH > VH) or other differences at the SC-CA1 circuit level along the dorsoventral axis.

Absence of 6× 1:4 t-LTP induction under complete blockade of GABAergic inhibition in IH and VH (compare Figures 7C and 7E) could be explained by two separate mechanisms (compare Figure S9).

In the first scenario (at the network level), complete blockade of GABAergic inhibition will suppress $GABA_B$ autoreceptor regulation of interneurons, such that the level of released GABA will increase, thereby counteracting CA1 neuron and DA fiber depolarization. This reduces DA release,[11] and glutamate release from SC axons, thereby counteracting depolarization of postsynaptic CA1 cells. This is consistent with evidence that insertion of new AMPARs into the postsynaptic membrane is promoted by D1 and D2 receptor signaling.[31] Thus, reduction of DA release can reduce the magnitude of 6× 1:4 t-LTP. In DH of rats, the extracellular dopamine concentration was shown to be 10-fold higher compared to VH and IH.[15] This would explain efficient induction of 6× 1:4 t-LTP under complete block of GABAergic inhibition in DH.

In the second scenario (at cellular level), two possible mechanisms need to be considered. First, $GABA_B$R activation has been shown to enhance mGluR activity,[95,96] which plays an essential role for 6× 1:4 t-LTP.[31] Secondly, $GABA_B$R activation promotes through cross talk with mGluRs insertion of new AMPARs into the postsynaptic membrane.[97] Since we previously proved insertion of cp-AMPARs and insertion of GluA2 containing new AMPARs to be instrumental for postsynaptic expression of low repeat t-LTP,[31] this $GABA_B$R effect might be essential for expression of 6× 1:4 t-LTP.

In summary, intrinsic excitability of CA1 PCs, and their response to synaptic input contribute to the functional diversity of CA1 PCs along the longitudinal axis of the hippocampus. We found higher basal glutamate release probability and higher CA1 PC excitability in VH, possibly arising from weaker GABAergic inhibition in this region. Correspondingly, the magnitude of t-LTP was smaller in VH than in IH and DH. DH showed stronger $GABA_B$ receptor mediated inhibition than VH and IH, and seems to be more resistant to t-LTP induction, but when induced it tends to be stronger. In contrast, VH may be more susceptible to t-LTP induction, but the t-LTP induced tends to be weaker. Pre- and postsynaptic mechanisms of t-LTP expression also varied depending on presence of GABAergic inhibition.

Thinking in terms of physiological relevance of low repeat t-LTP protocols, it is important to judge its properties when GABAergic inhibition is intact, which is the condition *in vivo*. Here, the 6× 1:1 t-LTP only worked in VH, while 6× 1:4 t-LTP was functional in all three regions. This complex interplay of excitation, inhibition, and possibly neuromodulation creates a unique processing platform in each hippocampal region, allowing for the formation of distinct types of memories along the dorsoventral axis.

Limitations of the study

In the present study, putative miniature EPSCs (pmEPSCs) were routinely recorded prior and after induction of t-LTP. This was done in the absence of TTX to avoid interference with t-LTP induction and expression. We can therefore not rule out that pmEPSCs were contaminated by some AP induced evoked EPSCs or that we missed some mEPSCs that were larger in amplitude than 20 pA.

STAR★METHODS

Detailed methods are provided in the online version of this paper and include the following:

- KEY RESOURCES TABLE
- RESOURCE AVAILABILITY
  - Lead contact
  - Materials availability
  - Data and code availability
- EXPERIMENTAL MODEL AND STUDY PARTICIPANT DETAILS
- METHOD DETAILS
  - Preparation of hippocampal slices
  - Electrophysiological recordings
  - Induction of spike timing-dependent plasticity
  - Data acquisition and data analysis
- QUANTIFICATION AND STATISTICAL ANALYSIS

SUPPLEMENTAL INFORMATION

Supplemental information can be found online at https://doi.org/10.1016/j.isci.2024.109320.

ACKNOWLEDGMENTS

Funding for this study was provided by: Federal State Saxony-Anhalt and the European Structural and Investment Funds (ESF, 2014–2020) (ZS/2016/08/80645) (ABINEP) to V.L.; DFG (ED 280/1-1 to E.E), (SFB779/B06, CRC1436/A06 to V.L.); Federal State of Saxony-Anhalt and the European Regional Developmental Fund (ERDF 2014–2020), Project: Center for Behavioral Brain Sciences (CBBS) (FKS: ZS/2016/04/78113) to E.E. and V.L.; German Center for Mental Health (DZPG) funded by BMBF and Federal State Saxony-Anhalt (FKZ: 01EE2305D) to V.L.

The authors thank Dr. Martin Both for providing Python code to analyze charge transfer, Regina Ziegler for excellent technical assistance, and Dr. Thomas Munsch for experimental suggestions and critical reading of the manuscript.

AUTHOR CONTRIBUTIONS

Conceptualization: V.L., E.E., and B.K.; Methodology: V.L., E.E., and B.K.; Investigation and formal analysis: B.K.; E.E., and V.L; Writing: V.L., B.K., and E.E.; Funding Acquisition: V.L. and E.E.; Resources: V.L.; Supervision: E.E. and V.L..

DECLARATION OF INTERESTS

The authors declare no competing interests.

Received: April 7, 2023
Revised: January 25, 2024
Accepted: February 20, 2024
Published: February 22, 2024

REFERENCES

1. Hughes, K.R. (1965). Dorsal and ventral hippocampus lesions and maze learning: influence of preoperative environment. Can. J. Psychol. *19*, 325–332.
2. Stevens, R., and Cowey, A. (1973). Effects of dorsal and ventral hippocampal lesions on spontaneous alternation, learned alternation and probability learning in rats. Brain Res. *52*, 203–224.
3. Strange, B.A., Witter, M.P., Lein, E.S., and Moser, E.I. (2014). Functional organization of the hippocampal longitudinal axis. Nat. Rev. Neurosci. *15*, 655–669.
4. Roth, T.C., and Pravosudov, V.V. (2009). Hippocampal volumes and neuron numbers increase along a gradient of environmental harshness: a large-scale comparison. Proc. Biol. Sci. *276*, 401–405.
5. Meis, S., Endres, T., and Lessmann, V. (2020). Neurotrophin signalling in amygdala-dependent cued fear learning. Cell Tissue Res. *382*, 161–172.
6. Dougherty, K.A., Islam, T., and Johnston, D. (2012). Intrinsic excitability of CA1 pyramidal neurones from the rat dorsal and ventral hippocampus. J. Physiol. *590*, 5707–5722.
7. Dubovyk, V., and Manahan-Vaughan, D. (2018). Less means more: The magnitude of synaptic plasticity along the hippocampal dorso-ventral axis is inversely related to the expression levels of plasticity-related neurotransmitter receptors. Hippocampus *28*, 136–150.
8. Milior, G., Di Castro, M.A., Pepe'Sciarria, L., Garofalo, S., Branchi, I., Ragozzino, D., Limatola, C., and Maggi, L. (2016). Electrophysiological properties of CA1 pyramidal neurons along the longitudinal axis of the mouse hippocampus. Sci. Rep. *6*, 38242–38249.

9. Bourne, J.N., and Harris, K.M. (2011). Coordination of size and number of excitatory and inhibitory synapses results in a balanced structural plasticity along mature hippocampal CA1 dendrites during LTP. Hippocampus *21*, 354–373.
10. Liu, G. (2004). Local structural balance and functional interaction of excitatory and inhibitory synapses in hippocampal dendrites. Nat. Neurosci. *7*, 373–379.
11. Santiago, M., Machado, A., and Cano, J. (1993). Regulation of the prefrontal cortical dopamine release by GABAA and GABAB receptor agonists and antagonists. Brain Res. *630*, 28–31.
12. Edelmann, E., and Lessmann, V. (2018). Dopaminergic innervation and modulation of hippocampal networks. Cell Tissue Res. *373*, 711–727.
13. Pawlak, V., Wickens, J.R., Kirkwood, A., and Kerr, J.N.D. (2010). Timing is not everything: neuromodulation opens the STDP gate. Front. Synaptic Neurosci. *2*, 146.
14. Brzosko, Z., Zannone, S., Schultz, W., Clopath, C., and Paulsen, O. (2017). Sequential neuromodulation of Hebbian plasticity offers mechanism for effective reward-based navigation. Elife *6*, e27756. https://doi.org/10.7554/eLife.27756.
15. Ishikawa, K., Ott, T., and McGaugh, J.L. (1982). Evidence for dopamine as a transmitter in dorsal hippocampus. Brain Res. *232*, 222–226.
16. Dubovyk, V., and Manahan-Vaughan, D. (2019). Gradient of expression of dopamine D2 receptors along the dorso-ventral axis of the hippocampus. Front. Synaptic Neurosci. *11*, 28.
17. Yao, H., and Dan, Y. (2001). Stimulus timing-dependent plasticity in cortical processing of orientation. Neuron *32*, 315–323.
18. Dan, Y., and Poo, M.-m. (2004). Spike timing-dependent plasticity of neural circuits. Neuron *44*, 23–30.
19. Zhang, L.I., Tao, H.W., Holt, C.E., Harris, W.A., and Poo, M. (1998). A critical window for cooperation and competition among developing retinotectal synapses. Nature *395*, 37–44.
20. Markram, H., Lübke, J., Frotscher, M., and Sakmann, B. (1997). Regulation of synaptic efficacy by coincidence of postsynaptic APs and EPSPs. Science *275*, 213–215.
21. Sjöström, P.J., Rancz, E.A., Roth, A., and Häusser, M. (2008). Dendritic excitability and synaptic plasticity. Physiol. Rev. *88*, 769–840.
22. Mizusaki, B.E.P., Li, S.S.Y., Costa, R.P., and Sjöström, P.J. (2022). Pre-and postsynaptically expressed spike-timing-dependent plasticity contribute differentially to neuronal learning. PLoS Comput. Biol. *18*, e1009409.
23. Fino, E., Paille, V., Cui, Y., Morera-Herreras, T., Deniau, J.M., and Venance, L. (2010). Distinct coincidence detectors govern the corticostriatal spike timing-dependent plasticity. J. Physiol. *588*, 3045–3062.
24. Kwag, J., and Paulsen, O. (2009). Bidirectional control of spike timing by GABA(A) receptor-mediated inhibition during theta oscillation in CA1 pyramidal neurons. Neuroreport *20*, 1209–1213. https://doi.org/10.1097/WNR.0b013e32832f5cc7.
25. Andrade-Talavera, Y., Duque-Feria, P., Paulsen, O., and Rodríguez-Moreno, A. (2016). Presynaptic Spike Timing-Dependent Long-Term Depression in the Mouse Hippocampus. Cereb. Cortex *26*, 3637–3654. https://doi.org/10.1093/cercor/bhw172.
26. Bouvier, G., Larsen, R.S., Rodríguez-Moreno, A., Paulsen, O., and Sjöström, P.J. (2018). Towards resolving the presynaptic NMDA receptor debate. Curr. Opin. Neurobiol. *51*, 1–7. https://doi.org/10.1016/j.conb.2017.12.020.
27. Larsen, R.S., Smith, I.T., Miriyala, J., Han, J.E., Corlew, R.J., Smith, S.L., and Philpot, B.D. (2014). Synapse-specific control of experience-dependent plasticity by presynaptic NMDA receptors. Neuron *83*, 879–893. https://doi.org/10.1016/j.neuron.2014.07.039.
28. Martínez-Gallego, I., Pérez-Rodríguez, M., Coatl-Cuaya, H., Flores, G., and Rodríguez-Moreno, A. (2022). Adenosine and astrocytes determine the developmental dynamics of spike timing-dependent plasticity in the somatosensory cortex. J. Neurosci. *42*, 6038–6052. https://doi.org/10.1523/JNEUROSCI.0115-22.2022.
29. Pérez-Rodríguez, M., Arroyo-García, L.E., Prius-Mengual, J., Andrade-Talavera, Y., Armengol, J.A., Pérez-Villegas, E.M., Duque-Feria, P., Flores, G., and Rodríguez-Moreno, A. (2019). Adenosine Receptor-Mediated Developmental Loss of Spike Timing-Dependent Depression in the Hippocampus. Cereb. Cortex *29*, 3266–3281. https://doi.org/10.1093/cercor/bhy194.
30. Rodríguez-Moreno, A., and Paulsen, O. (2008). Spike timing-dependent long-term depression requires presynaptic NMDA receptors. Nat. Neurosci. *11*, 744–745. https://doi.org/10.1038/nn.2125.
31. Cepeda-Prado, E.A., Khodaie, B., Quiceno, G.D., Beythien, S., Edelmann, E., and Lessmann, V. (2022). Calcium-Permeable AMPA Receptors Mediate Timing-Dependent LTP Elicited by Low Repeat Coincident Pre-and Postsynaptic Activity at Schaffer Collateral-CA1 Synapses. Cereb. Cortex *32*, 1682–1703.
32. Edelmann, E., Cepeda-Prado, E., Franck, M., Lichtenecker, P., Brigadski, T., and Leßmann, V. (2015). Theta burst firing recruits BDNF release and signaling in postsynaptic CA1 neurons in spike-timing-dependent LTP. Neuron *86*, 1041–1054.
33. Wei, C.-l., Liu, Y.-h., Yang, M.-h., Liu, Z.-q., and Ren, W. (2013). Dopamine inhibits high-frequency stimulation-induced long-term potentiation of intrinsic excitability in CA1 hippocampal pyramidal neurons. Neurosignals *21*, 150–159.
34. Papatheodoropoulos, C., and Kostopoulos, G. (2000). Dorsal-ventral differentiation of short-term synaptic plasticity in rat CA1 hippocampal region. Neurosci. Lett. *286*, 57–60.
35. Bender, V.A., Pugh, J.R., and Jahr, C.E. (2009). Presynaptically expressed long-term potentiation increases multivesicular release at parallel fiber synapses. J. Neurosci. *29*, 10974–10978.
36. Pandis, C., Sotiriou, E., Kouvaras, E., Asprodini, E., Papatheodoropoulos, C., and Angelatou, F. (2006). Differential expression of NMDA and AMPA receptor subunits in rat dorsal and ventral hippocampus. Neuroscience *140*, 163–175.
37. Wyllie, D.J.A., Livesey, M.R., and Hardingham, G.E. (2013). Influence of GluN2 subunit identity on NMDA receptor function. Neuropharmacology *74*, 4–17.
38. Shi, S., Hayashi, Y., Esteban, J.A., and Malinow, R. (2001). Subunit-specific rules governing AMPA receptor trafficking to synapses in hippocampal pyramidal neurons. Cell *105*, 331–343.
39. Faber, D.S., and Korn, H. (1991). Applicability of the coefficient of variation method for analyzing synaptic plasticity. Biophys. J. *60*, 1288–1294. https://doi.org/10.1016/S0006-3495(91)82162-2.
40. Manabe, T., Wyllie, D.J., Perkel, D.J., and Nicoll, R.A. (1993). Modulation of synaptic transmission and long-term potentiation: effects on paired pulse facilitation and EPSC variance in the CA1 region of the hippocampus. J. Neurophysiol. *70*, 1451–1459. https://doi.org/10.1152/jn.1993.70.4.1451.
41. Brock, J.A., Thomazeau, A., Watanabe, A., Li, S.S.Y., and Sjöström, P.J. (2020). A Practical Guide to Using CV Analysis for Determining the Locus of Synaptic Plasticity. Front. Synaptic Neurosci. *12*, 11. https://doi.org/10.3389/fnsyn.2020.00011.
42. Malinow, R., and Tsien, R.W. (1990). Presynaptic enhancement shown by whole-cell recordings of long-term potentiation in hippocampal slices. Nature *346*, 177–180. https://doi.org/10.1038/346177a0.
43. Glasgow, S.D., McPhedrain, R., Madranges, J.F., Kennedy, T.E., and Ruthazer, E.S. (2019). Approaches and Limitations in the Investigation of Synaptic Transmission and Plasticity. Front. Synaptic Neurosci. *11*, 20. https://doi.org/10.3389/fnsyn.2019.00020.
44. Isaac, J.T., Nicoll, R.A., and Malenka, R.C. (1995). Evidence for silent synapses: implications for the expression of LTP. Neuron *15*, 427–434. https://doi.org/10.1016/0896-6273(95)90046-2.
45. Isaac, J.T., Oliet, S.H., Hjelmstad, G.O., Nicoll, R.A., and Malenka, R.C. (1996). Expression mechanisms of long-term potentiation in the hippocampus. J. Physiol. Paris *90*, 299–303. https://doi.org/10.1016/s0928-4257(97)87901-6.
46. Kerchner, G.A., and Nicoll, R.A. (2008). Silent synapses and the emergence of a postsynaptic mechanism for LTP. Nat. Rev. Neurosci. *9*, 813–825. https://doi.org/10.1038/nrn2501.
47. Liao, D., Hessler, N.A., and Malinow, R. (1995). Activation of postsynaptically silent synapses during pairing-induced LTP in CA1 region of hippocampal slice. Nature *375*, 400–404. https://doi.org/10.1038/375400a0.
48. Isaacson, J.S., Solís, J.M., and Nicoll, R.A. (1993). Local and diffuse synaptic actions of GABA in the hippocampus. Neuron *10*, 165–175.
49. Sallard, E., Letourneur, D., and Legendre, P. (2021). Electrophysiology of ionotropic GABA receptors. Cell. Mol. Life Sci. *78*, 5341–5370.
50. Fink, A.E., Sariñana, J., Gray, E.E., and O'dell, T.J. (2007). Activity-dependent depression of local excitatory connections in the CA1 region of mouse hippocampus. J. Neurophysiol. *97*, 3926–3936.
51. Price, C.J., Scott, R., Rusakov, D.A., and Capogna, M. (2008). GABAB receptor modulation of feedforward inhibition through hippocampal neurogliaform cells. J. Neurosci. *28*, 6974–6982.
52. Petrides, T., Georgopoulos, P., Kostopoulos, G., and Papatheodoropoulos, C. (2007). The GABA A receptor-mediated recurrent inhibition in ventral compared with dorsal CA1 hippocampal region is weaker, decays faster and lasts less. Exp. Brain Res. *177*, 370–383.
53. Papatheodoropoulos, C., Asprodini, E., Nikita, I., Koutsona, C., and Kostopoulos, G.

(2002). Weaker synaptic inhibition in CA1 region of ventral compared to dorsal rat hippocampal slices. Brain Res. *948*, 117–121.
54. Lenz, R.A., Pitler, T.A., and Alger, B.E. (1997). High intracellular Cl− concentrations depress G-protein-modulated ionic conductances. J. Neurosci. *17*, 6133–6141.
55. Marcelin, B., Liu, Z., Chen, Y., Lewis, A.S., Becker, A., McClelland, S., Chetkovich, D.M., Migliore, M., Baram, T.Z., Esclapez, M., and Bernard, C. (2012). Dorsoventral differences in intrinsic properties in developing CA1 pyramidal cells. J. Neurosci. *32*, 3736–3747.
56. Mizuseki, K., Diba, K., Pastalkova, E., and Buzsáki, G. (2011). Hippocampal CA1 pyramidal cells form functionally distinct sublayers. Nat. Neurosci. *14*, 1174–1181.
57. Derchansky, M., Shahar, E., Wennberg, R.A., Samoilova, M., Jahromi, S.S., Abdelmalik, P.A., Zhang, L., and Carlen, P.L. (2004). Model of frequent, recurrent, and spontaneous seizures in the intact mouse hippocampus. Hippocampus *14*, 935–947.
58. Papatheodoropoulos, C., Moschovos, C., and Kostopoulos, G. (2005). Greater contribution of N-methyl-D-aspartic acid receptors in ventral compared to dorsal hippocampal slices in the expression and long-term maintenance of epileptiform activity. Neuroscience *135*, 765–779.
59. Zemankovics, R., Káli, S., Paulsen, O., Freund, T.F., and Hájos, N. (2010). Differences in subthreshold resonance of hippocampal pyramidal cells and interneurons: the role of h-current and passive membrane characteristics. J. Physiol. *588*, 2109–2132.
60. Marcelin, B., Lugo, J.N., Brewster, A.L., Liu, Z., Lewis, A.S., McClelland, S., Chetkovich, D.M., Baram, T.Z., Anderson, A.E., Becker, A., et al. (2012). Differential dorso-ventral distributions of Kv4. 2 and HCN proteins confer distinct integrative properties to hippocampal CA1 pyramidal cell distal dendrites. J. Biol. Chem. *287*, 17656–17661.
61. Daoudal, G., and Debanne, D. (2003). Long-term plasticity of intrinsic excitability: learning rules and mechanisms. Learn. Mem. *10*, 456–465.
62. Haring, J.H., and Davis, J.N. (1985). Differential distribution of locus coeruleus projections to the hippocampal formation: anatomical and biochemical evidence. Brain Res. *325*, 366–369.
63. Dodt, H.-U., Pawelzik, H., and Zieglgänsberger, W. (1991). Actions of noradrenaline on neocortical neurons in vitro. Brain Res. *545*, 307–311.
64. Monyer, H., Burnashev, N., Laurie, D.J., Sakmann, B., and Seeburg, P.H. (1994). Developmental and regional expression in the rat brain and functional properties of four NMDA receptors. Neuron *12*, 529–540.
65. Sholl, D.A. (1953). Dendritic organization in the neurons of the visual and motor cortices of the cat. J. Anat. *87*, 387–406.
66. Malik, R., Dougherty, K.A., Parikh, K., Byrne, C., and Johnston, D. (2016). Mapping the electrophysiological and morphological properties of CA 1 pyramidal neurons along the longitudinal hippocampal axis. Hippocampus *26*, 341–361.
67. Mainen, Z.F., and Sejnowski, T.J. (1996). Influence of dendritic structure on firing pattern in model neocortical neurons. Nature *382*, 363–366.
68. Papatheodoropoulos, C., and Kouvaros, S. (2016). High-frequency stimulation-induced synaptic potentiation in dorsal and ventral CA1 hippocampal synapses: the involvement of NMDA receptors, mGluR5, and (L-type) voltage-gated calcium channels. Learn. Mem. *23*, 460–464.
69. Martens, U., Capito, B., and Wree, A. (1998). Septotemporal distribution of [3H] MK-801,[3H] AMPA and [3H] Kainate binding sites in the rat hippocampus. Anat. Embryol. *198*, 195–204.
70. Santiago, M., Machado, A., and Cano, J. (1993). Regulation of prefrontal cortical dopamine release by dopamine receptor agonists and antagonists. Eur. J. Pharmacol. *239*, 83–91.
71. Okun, M., and Lampl, I. (2009). Balance of excitation and inhibition. Scholarpedia *4*, 7467.
72. Kirkwood, A. (2015). Balancing excitation and inhibition. Neuron *86*, 348–350.
73. Paille, V., Fino, E., Du, K., Morera-Herreras, T., Perez, S., Kotaleski, J.H., and Venance, L. (2013). GABAergic circuits control spike-timing-dependent plasticity. J. Neurosci. *33*, 9353–9363.
74. Ruiz, A., Fabian-Fine, R., Scott, R., Walker, M.C., Rusakov, D.A., and Kullmann, D.M. (2003). GABAA receptors at hippocampal mossy fibers. Neuron *39*, 961–973.
75. Pugh, J.R., and Jahr, C.E. (2011). Axonal GABAA receptors increase cerebellar granule cell excitability and synaptic activity. J. Neurosci. *31*, 565–574.
76. Wang, L., Kloc, M., Maher, E., Erisir, A., and Maffei, A. (2019). Presynaptic GABAA receptors modulate thalamocortical inputs in layer 4 of rat V1. Cereb. Cortex *29*, 921–936.
77. Jackson, M.B., and Zhang, S.J. (1995). Action potential propagation and propagation block by GABA in rat posterior pituitary nerve terminals. J. Physiol. *483*, 597–611.
78. Stell, B.M., Rostaing, P., Triller, A., and Marty, A. (2007). Activation of presynaptic GABAA receptors induces glutamate release from parallel fiber synapses. J. Neurosci. *27*, 9022–9031.
79. Zorrilla de San Martin, J., Trigo, F.F., and Kawaguchi, S.y. (2017). Axonal GABAA receptors depolarize presynaptic terminals and facilitate transmitter release in cerebellar Purkinje cells. J. Physiol. *595*, 7477–7493.
80. Edelmann, E., and Lessmann, V. (2011). Dopamine modulates spike timing-dependent plasticity and action potential properties in CA1 pyramidal neurons of acute rat hippocampal slices. Front. Synaptic Neurosci. *3*, 6.
81. Edelmann, E., and Lessmann, V. (2013). Dopamine regulates intrinsic excitability thereby gating successful induction of spike timing-dependent plasticity in CA1 of the hippocampus. Front. Neurosci. *7*, 25. https://doi.org/10.3389/fnins.2013.00025.
82. Zucker, R.S., and Regehr, W.G. (2002). Short-term synaptic plasticity. Annu. Rev. Physiol. *64*, 355–405.
83. Seabrook, G.R., Easter, A., Dawson, G.R., and Bowery, B.J. (1997). Modulation of long-term potentiation in CA1 region of mouse hippocampal brain slices by GABAA receptor benzodiazepine site ligands. Neuropharmacology *36*, 823–830.
84. Shen, H.-Y., Canas, P.M., Garcia-Sanz, P., Lan, J.-Q., Boison, D., Moratalla, R., Cunha, R.A., and Chen, J.-F. (2013). Adenosine A2A receptors in striatal glutamatergic terminals and GABAergic neurons oppositely modulate psychostimulant action and DARPP-32 phosphorylation. PLoS One *8*, e80902.
85. Gaiarsa, J.-L., Caillard, O., and Ben-Ari, Y. (2002). Long-term plasticity at GABAergic and glycinergic synapses: mechanisms and functional significance. Trends Neurosci. *25*, 564–570.
86. Collingridge, G.L., Isaac, J.T.R., and Wang, Y.T. (2004). Receptor trafficking and synaptic plasticity. Nat. Rev. Neurosci. *5*, 952–962.
87. Kantamneni, S. (2015). Cross-talk and regulation between glutamate and GABAB receptors. Front. Cell. Neurosci. *9*, 135.
88. Olpe, H.R., and Karlsson, G. (1990). The effects of baclofen and two GABAB-receptor antagonists on long-term potentiation. Naunyn-Schmiedeberg's Arch. Pharmacol. *342*, 194–197.
89. Brucato, F.H., Levin, E.D., Mott, D.D., Lewis, D.V., Wilson, W.A., and Swartzwelder, H.S. (1996). Hippocampal long-term potentiation and spatial learning in the rat: effects of GABAB receptor blockade. Neuroscience *74*, 331–339.
90. Mott, D.D., and Lewis, D.V. (1991). Facilitation of the induction of long-term potentiation by GABAB receptors. Science *252*, 1718–1720.
91. Davies, C.H., Starkey, S.J., Pozza, M.F., and Collingridge, G.L. (1991). GABA B autoreceptors regulate the induction of LTP. Nature *349*, 609–611.
92. Freund, T.F., and Katona, I. (2007). Perisomatic inhibition. Neuron *56*, 33–42.
93. Elfant, D., Pál, B.Z., Emptage, N., and Capogna, M. (2008). Specific inhibitory synapses shift the balance from feedforward to feedback inhibition of hippocampal CA1 pyramidal cells. Eur. J. Neurosci. *27*, 104–113.
94. Liang, S.-L., Carlson, G.C., and Coulter, D.A. (2006). Dynamic regulation of synaptic GABA release by the glutamate-glutamine cycle in hippocampal area CA1. J. Neurosci. *26*, 8537–8548.
95. Hirono, M., Yoshioka, T., and Konishi, S. (2001). GABAB receptor activation enhances mGluR-mediated responses at cerebellar excitatory synapses. Nat. Neurosci. *4*, 1207–1216.
96. Rives, M.L., Vol, C., Fukazawa, Y., Tinel, N., Trinquet, E., Ayoub, M.A., Shigemoto, R., Pin, J.P., and Prézeau, L. (2009). Crosstalk between GABAB and mGlu1a receptors reveals new insight into GPCR signal integration. EMBO J. *28*, 2195–2208.
97. Kelly, L., Farrant, M., and Cull-Candy, S.G. (2009). Synaptic mGluR activation drives plasticity of calcium-permeable AMPA receptors. Nat. Neurosci. *12*, 593–601.
98. Tidball, P., Burn, H.V., Teh, K.L., Volianskis, A., Collingridge, G.L., and Fitzjohn, S.M. (2017). Differential ability of the dorsal and ventral rat hippocampus to exhibit group I metabotropic glutamate receptor–dependent synaptic and intrinsic plasticity. Brain Neurosci. Adv. *1*, 2398212816689792.
99. Bekkers, J.M., and Stevens, C.F. (1990). Presynaptic mechanism for long-term potentiation in the hippocampus. Nature *346*, 724–729. https://doi.org/10.1038/346724a0.

STAR★METHODS

KEY RESOURCES TABLE

REAGENT or RESOURCE	SOURCE	IDENTIFIER
Chemicals, peptides, and recombinant proteins		
Picrotoxin	Sigma Aldrich	Cat # P1675
CGP 55845 hydrochloride	Tocris	Cat # 1248/10
Isofluran	cp-pharma	Cat # 1214
Experimental models: organisms/strains		
Mouse: C57Bl/6J (WT)	Charles River/Laboratories	C57Bl/6J
Software and algorithms		
Patchmaster	HEKA Elektronik	http://www.heka.com/products/products_main.html
Fitmaster	HEKA Elektronik	https://www.heka.com/downloads/downloads_main.html
Minianalysis	Synaptosoft	https://synaptosoft.softwareinformer.com
Graph Pad Prism 8	GraphPad Software	https://www.graphpad.com/scientificsoftware/prism/
Corel Draw	Corel Graphics Suite	http://www.coreldraw.com/us/
Origin	OriginLab Corporation	http://www.orginlab.com/index.aspx?go=
Python 3.11	This study	Available upon request
Other		
Vibratome	Leica	https://www.leicabiosystems.com/es/equipo-histologia/microtomos-deslizantes/microtomos-de-cuchillas-vibrantes/leica-vt1200-s/

RESOURCE AVAILABILITY

Lead contact

- Further information and requests for resources and reagents should be directed to and will be fulfilled by the Lead Contact, Volkmar Leßmann (volkmar.lessmann@med.ovgu.de).

Materials availability

This study did not generate new unique reagents.

Data and code availability

- Data reported in this paper will be shared by the lead contact upon reasonable request.
- This paper does not report original code.
- Any additional information required to reanalyze the data reported in this paper is available from the lead contact upon request.

EXPERIMENTAL MODEL AND STUDY PARTICIPANT DETAILS

All experiments were performed according to the ethical guidelines for using animals inexperiments and were carried out following the European Committee Council Directive (2010/63/EU) and approved by the local animal care committee (LandesverwaltungsamtSachsen-Anhalt). C57Bl6/J adult male mice (RRID: MGI: 2159965) were housed in a temperature-controlled environment with a 12-hour light/dark cycle and fed *ad libitum*.

METHOD DETAILS

Preparation of hippocampal slices

All experiments were performed according to the ethical guidelines for using animals in experiments and were carried out following the European Committee Council Directive (2010/63/EU) and approved by the local animal care committee (Landesverwaltungsamt Sachsen-Anhalt). Two different cutting methods were used to obtain acute hippocampal slices from male C57Bl/6J mice (Charles River, Germany; postnatal day P29-P32, own breeding). We did not extract hippocampi but rather used intact cortical hemispheres and applied two different

cutting planes, including sagittal cuttings to obtain dorsal hippocampal slices (DH), and transversal cuts for intermediate (IH, early slices) and ventral slices (VH, late slices).

Briefly, animals were deeply anesthetized using forene (Isofluran CP, cp-pharma, Germany) before decapitation. The brain was rapidly dissected and transferred into ice-cold artificial cerebrospinal fluid (ACSF) cutting solution containing (in mM): 125 NaCl, 2.5 KCl, 26 $NaHCO_3$, 0.8 NaH_2PO_4, 25 glucose, 6 $MgCl_2$, 1 $CaCl_2$, saturated with 95% O_2 and 5% CO_2 (pH 7.2-7.4; 303-305 mOsmol/kg). Sagittal cuts: after chilling the brain in ice-cold solution, the hemispheres were separated by a sagittal cut along the midline. Each hemisphere was then medially mounted onto the stage and sliced (350 μm thickness) starting from the lateral surface parallel to the sagittal plane (caudal to rostral cutting direction) to obtain sagittal slices for the DH[98] using a vibratome (VT 1200 S, Leica, Germany). Transversal cuts: to obtain IH and VH slices, the complete brain with both hemispheres containing the hippocampus and the entorhinal cortex was glued on the ventral side and transversal cuts started from caudal pole (350 μm thick sections). After slicing, a cut with a surgical blade in CA2, perpendicular to the surface of the slices, was used to abrogate excessive CA3 input to the CA1 region, to prevent epileptiform activity originating from CA3 inputs. Slices were then transferred to a handmade interface chamber containing prewarmed cutting solution and incubated for 25 min at 32°C. After warming up, the chamber was transferred to room temperature (~21°C) for at least 1 hour before individual slices were transferred to the recording chamber.[32]

After recovery at room temperature, whole cell patch-clamp recordings were performed from CA1 pyramidal neurons of submerged slices continuously perfused (1-2 ml per min) with pre-warmed (30 ± 0.2°C) carboxygenated (5% CO_2, 95% O_2) physiological ACSF solution (125 mM NaCl, 2.5 mM KCl, 0.8 mM NaH_2PO_4, 25 mM $NaHCO_3$, 25 mM Glucose, 1 mM $MgCl_2$, 2 mM $CaCl_2$; pH 7.4; 301-303 mOsmol/kg).

For blockade of only $GABA_A$ receptor mediated inhibition, picrotoxin (100 μM; Sigma Aldrich) was added to the recording ACSF solution. For complete blockade of GABAergic responses, the $GABA_B$ receptor inhibitor CGP 55845 hydrochloride (10 μM; Tocris, Germany) was added to the picrotoxin containing ACSF.

Electrophysiological recordings

Individual pyramidal neurons in the CA1 region (along the dorso-ventral axis) of acute hippocampal slices were visualized with DIC infrared video microscopy (RT-SE series camera; Diagnostic instruments, Michigan, USA) for whole-cell patch-clamp recordings. The glass pipettes (resistance 4-6 MΩ) were filled with an internal solution containing (in mM): 10 HEPES, 20 KCl, 115 potassium gluconate, 10 Na phosphocreatine, 0.3 Na-GTP, and 4 Mg-ATP (pH 7.4, 285-290 mOsmol/kg) to patch the cells. This combination of solutions gave rise to a liquid junction potential of +10 mV that was corrected for in all recordings. Cells were held at -70 mV in the current clamp or voltage clamp mode of an EPC-8 patch-clamp amplifier (HEKA, Lambrecht, Germany). A focal glass stimulation pipette (resistance 0.7 – 0.9 MΩ) containing recording ACSF was placed in the stratum radiatum of the CA1 subfield to generate an excitatory postsynaptic potential (EPSP, at 0.05 Hz) at SC-CA1 synapses. The stimulus intensity was adjusted to evoke EPSP amplitudes of 4-5 mV corresponding to 30%–50% of maximal EPSP amplitudes (stimulus duration 0.7 ms, intensity 90 to 700 μA).

Induction of spike timing-dependent plasticity

To induce t-LTP with spike timing-dependent plasticity (STDP) protocols, an individual EPSP, generated by focal extracellular stimulation of SC fibers was paired, with a single postsynaptic action potential (AP) or with a burst of 4 APs (at 200 Hz) induced by somatic current injection (2 ms; 1 nA) through the recording electrode (for more details, see.[32] Spike timing intervals (Δt) were measured as the time between the onset of evoked EPSP and the peak of the first action potential (set to +10 ms). Pairing was repeated six times at a frequency of 0.5 Hz to induce 6× 1:1 or 6× 1:4 timing-dependent (t)-LTP.[31] EPSPs were elicited every 20 s (i.e., 0.05 Hz) for 10 minutes baseline and then 30 minutes after STDP induction. A separate group of cells was used to assess possible spontaneous changes in synaptic transmission (stimulation at 0.05 Hz for 40 min) without any STDP stimulation and served as unpaired negative controls (designated as 0:0 controls).

Data acquisition and data analysis

Whole-cell recordings were obtained using a patch-clamp amplifier (EPC-8, HEKA, Germany) connected to a LiH8 + 8 interface. Data were filtered at 3 kHz and digitized at 10 kHz using PATCH MASTER software (HEKA, Germany). Data analysis was performed using FITMASTER (HEKA, Germany). Current clamp mode at a holding potential of -70 mV was used in all experiments, except for the paired-pulse ratio (PPR), miniature EPSCs, as well as AMPAR/NMDAR current ratios which were recorded in the voltage-clamp mode at -70 mV and -20 mV (for NMDA current) holding potential. Of note, the liquid junction potential of +10 mV resulting from the combination of internal and external solutions was corrected. The mean of EPSP slope was calculated from the initial 2 ms after EPSP onset. Synaptic input/output curves were determined for each cell and SC stimulation for subsequent t-LTP induction was generally adjusted to stimulation strength yielding half-maximal EPSP amplitudes. Figure S4 shows the average EPSP slope and the average stimulation current required to obtain this half-maximal EPSP across all cells recorded under the same conditions for GABAergic inhibition. The baseline of synaptic responses before inducing STDP was set to 100 % (average over 10 min), and all EPSPs after induction of STDP were normalized to this baseline. Input resistance was controlled by hyperpolarizing current steps (250 ms; 20 pA), elicited prior to EPSP responses. The change of EPSP slopes was used to calculate synaptic strength as the average of EPSP slopes 20 to 30 min after t-LTP induction, divided by the mean EPSP slope measured during 10 min before STDP stimulation (baseline). Cells were only included for analysis if the initial resting membrane potential (RMP) was between -55 and -70 mV. Cells were excluded when the input resistance varied more than 30% over the entire experiment. Furthermore, cells showing visible "run-up" or "run-down" of EPSP slopes during baseline recording were excluded. Data were binned at 1 min intervals. For evaluation of changes in EPSP

rise-times (compare Figure S2) the average time from 10% to 90% of the peak EPSP amplitudes was calculated. The EPSP half-width was measured as the time between 50% of the peak EPSP amplitude on the rising and the decaying phase of the synaptic response.

The AMPAR/NMDAR current ratio was measured at the end of the EPSP recording after t-LTP induction as a read-out of AMPA receptor insertion after inducing t-LTP. In voltage clamp recordings, AMPA receptor-mediated components were determined as EPSC peak currents recorded at a holding potential of −70 mV. NMDAR-mediated current components were determined from EPSCs recorded at -20 mV holding potential. Due to distinct kinetics of NMDAR mediated EPSC components along the longitudinal axis of the hippocampus,[36] NMDAR components were read out as the remaining current amplitude at different time points after EPSC start (i.e. DH: 45 ms, IH and VH: 50 ms; compare Figure 4C). The AMPAR/NMDAR current ratio was calculated from these two amplitudes of the averaged EPSCs (3-5 sweeps) at respective holding.[37]

As an additional measure for possible differences in glutamate release probability, miniature excitatory postsynaptic currents (mEPSCs) were collected from 3 min of continuous recordings at -70 mV holding potential in voltage clamp (VC) mode before t-LTP induction. As previously described,[31] we analyzed with the Minianalysis program (Synaptosoft, USA) all small amplitude EPSCs (cut-off amplitude: 20 pA to minimize collection of AP-driven EPSCs) and named these events "putative" mEPSCs. Cumulative fraction plots for inter-event intervals (IEI) of putative mEPSCs and mean amplitudes were compared.[31]

Coefficient of variation analysis of evoked EPSPs in CA1 PC recordings was performed in CC mode at -70 mV holding potential as described for all t-LTP experiments. For each cell, the inverse of the squared coefficient of variation (1/CV2) of synaptic responses after induction of LTP (i.e., condition "a") is normalized to the respective value for 1/CV2 of the same cell during the 10 min of baseline recording (i.e., condition "b"). For each cell, this ratio is plotted on the y-axis against the normalized t-LTP magnitude (i.e., EPSP slope after compared to before LTP expression) of the same cell on the x-axis. Each open circle represents an individual cell. According to quantal analysis of synaptic transmission (compare[39,99]; for a recent review see[41]), cells with a position on or above the red line of unity (compare Figures S5 and S6) show LTP due to increased probability of transmitter release, while cells with a position underneath this line of unity are potentiated most likely by postsynaptic mechanisms (i.e., increased quantal size).

For charge transfer analysis of mEPSCs, a Python code was written that performed numerical integration of all recorded putative (m)EPSC of a given cell during 180 s recording time, thus yielding the corresponding transferred charge. From this single cell data, we calculated the mean transferred charge per CA1 PC in DH, IH, and VH.

QUANTIFICATION AND STATISTICAL ANALYSIS

Statistical analysis was performed using GraphPad Prism version 8.4 (GraphPad Software, USA) or OriginPro (OriginLab Corp., Northampton, MA, USA). Pooled experimental data from at least three different animals are expressed as mean ± SEM. In addition, the number of recorded cells (n) and the number of animals (N) are shown in the results section and in the figure legends. Shapiro-Wilk test was used to determine the distribution of variables. For normally distributed data, paired or unpaired two-tailed Student's t-tests were used to analyze data sets. To determine significance of t-LTP a paired Student's t-test was used to compare non-normalized baseline vs post-conditioning values. Otherwise, nonparametric Mann-Whitney U-test or Kolmogorov–Smirnov test for cumulative distribution was applied. Multiple comparisons were assessed with a one-way analysis of variance (ANOVA), followed by a post hoc t-test (Dunnett's test, or Kruskal–Wallis test), or followed by post hoc Dunn's test for parametric and nonparametric data, respectively. To assess multiple comparisons for datasets consisting of cumulative distribution plots we used ANOVA followed by Kruskal–Wallis post hoc t-test. A P-value <0.05 was set as level of significance and is indicated by an asterisk. The actual statistic procedures used for each experiment are mentioned in the text. Graphs were created using Corel Draw 2019.